Chapter 6
Localization of grouting faults in post tensioned concrete structures

Martin Krause[1]

1 Introduction

1.1 State of the art and existing guidelines and recommendations

The investigation of post-tensioned tendon ducts is one of the very important and fascinating testing problems for concrete structures. Much progress was achieved in the past two decades including multidisciplinary research. This includes large area measuring. The progress of research and development bases on four columns:

- Measurement and evaluation at large scale test specimens applying automated equipment
- Application at large scale post tensioned test specimens
- Reconstruction calculation for visualisation of results
- Modelling of elastic wave propagation for better understanding of effects.

The application of the methods is in an intermediate state between: practical application, validation, writing of recommendations and guidelines, even standards for certain methods, research for more reliable methods, development of automated methods for fast application.

This text is intended for a brief description of the state of the art of existing methods including some historical aspects of development of methods. There are other interesting publications of committees working on providing information and

[1]Other contributors to this chapter are: O. Abraham, L. Alver, D. Breysse, J.P. Balayssac, M. Forde, A. Kodjo, A. Moczko, C. G. Petersen, J. Popovics, F. Rivard.

M. Krause (✉)
BAM, Bundesanstalt für Materialforschung und –prüfung, Berlin, Germany
e-mail: martin.krause@bam.de

D. Breysse (ed.), *Non-Destructive Assessment of Concrete Structures: Reliability and Limits of Single and Combined Techniques*, RILEM State-of-the-Art Reports 1,
DOI 10.1007/978-94-007-2736-6_6, © RILEM 2012

explaining NDT methods for concrete in order bringing forward their application [Forde, 2006]. Additionally in the United Kingdom recommendations for design and tailing, duct and grouting systems as well as certification of post-tensioned operations and training are published. Details about overall design strategy and protection systems are outlined [Concrete Society, 2002].

Several groups of experts are also working on this topic: ACI 228, COFREND, DGZfP (German Soc. NDT, through its Technical Committee NDT-CE with its subcommittees and recommendations for ultrasonics, impact-echo, RADAR, radiography, quality assurance, education [DGZfP, 2010], COST Materials Action 534, dealing with Impact-Echo. The material published by these groups is considered for the present text as far as possible.

1.2 Fields of application

In principle there are three fields of application: regular inspection of prestressed structures, quality assurance of repair, quality assurance of new structures.

Grouting faults are appearing in all areas of tendon ducts, and there are many structures with large areas of ungrouted ducts [FDoT, 2003, Eichinger et al, 2000]. The regular damage assessment of bridges, which are planned to be demolished is a very important activity in this field [Vogel, 2002]. Following a technical report of the Concrete Society of the United Kingdom about 30 % of the post-tensioned concrete structures suffer from voids and ungrouted tendons [Concrete Society, 2002].

Many developed countries are active in this field. For instance, in Germany application of advanced NDT is part of Maintenance of Engineering Structures (BMS, Bauwerk-Management System) of Bundesanstalt für Straßenwesen (BASt, Federal Highway Research Institute). All state owned bridges are regularly inspected following the standard DIN 1078 (inspection interval 3 years and 6 years (general inspection). If there are some abnormalities, which cannot easily be classified, a so called OSA (*Objektbezogene Schadensanalyse*, Structure related Damage Analysis) takes place [BAsT, 2010]. Then NDT-CE-methods are applied by engineering offices or research institutes.

2 Overview of Methods

Principally the methods for assessing the grouting of metallic tendon ducts are divided in three groups:

- Radiography with X-rays and γ-Radiation (see § 3)
- Methods with mechanical waves, including impact-echo and ultrasonic methods (see § 4 to 6). There is a wide variety of techniques and variants, that will be detailed in the following. Mechanical wave methods are divided in Impact-Echo and Ultrasonic methods. Impact-Echo was the first mechanical wave method which was widely applied at prestressed concrete structures for testing post tensioned tendon ducts. Thus section 4 is dedicated to this subject.

- Development of broadband low frequency ultrasonic transducers and imaging techniques since the 1990 decade enable application of ultrasonic echo technique for concrete structures. These techniques (including ultrasonic through transmission) are described in sections 5 and 6. They are related to modelling and reconstruction techniques, which can only briefly mentioned in this state of the art [Langenberg et al, 2002], [Langenberg et al, 2009]
- Impulse radar, which can be used for plastic ducts (see § 7.1).

Transient thermography is widely applied in NDT. So it is obvious to apply it for concrete structures. There are encouraging results, but it seems that its application is restricted to the near surface region because of the relatively small penetration depth of the heating pulses in concrete. It will be briefly treated (see §7.2).

3 Radiography with X- and γ-Radiation

High energy electromagnetic waves were already applied in civil engineering in the nineteen-thirties for investigating welded joints. It is obvious that the best state-of-the-art technical solutions are always applied to prestressed concrete structures in order to achieve a contrast between grouted and voided regions. Current γ-radiography is sometimes used as reference method in addition to mechanical waves.

3.1 X-rays

Radiography with X-rays was already carried out in the thirties of last century for testing steel structures. However to investigate tendon ducts in concrete structures the penetration depth has to be large enough. This means energy of 320 keV and more for 20 cm thick concrete elements. For higher energy linear and circular accelerators are used with X-ray energy between 2 and 6 MeV.

With linear accelerators, even thicker concrete elements can be tested with γ-radiography. Since the source can easily be switched on and off the application is somewhere easier than the handling of the radiation sources. Applications at concrete bridges, which are around 1 m thick, are described in France [Duffay and Piccardi, 1985], [Lanneau, 1993].

3.2 Gamma-Radiation

The application of γ-radiography is performed in several modifications. There are two typical types of sources: Iridium 192 (up to 38 cm concrete) and Cobalt 60 (typically up to 60 cm concrete). The sensors are films or phosphor imaging plates. Guidelines are published e.g. in Germany [DGZfP, 1990] and France [AFNOR, 2011] or by international bodies [IAEA, 2002].

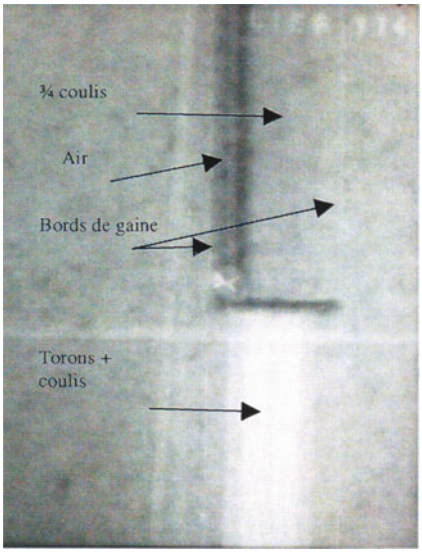

Fig. 6.1 Localisation of grouting faults with Gammagraphy in a specimen at CETE de Lyon (after [Roenelle and Abraham, 2006])

Fig. 6.2 Plastic tubes for Cobalt 60 source at Large Concrete Slab at BAM (after [Taffe et al, 2003])

The capability of Cobalt 60 sources is demonstrated at specimens constructed at BAM and LCPC Lyon (Figs. 6.1 to 6. 3) ([Roenelle and Abraham, 2006], [Taffe and al, 2003], [Krause et al, 2008]).

In Figs. 6.4 and 6.5 two examples are shown which demonstrate the capability of gammagraphy to localize ungrouted areas of tendon ducts, non-prestressed rebars and non tightened strands 0.

The sensitivity of phosphor imaging plates depends on the thickness of the phosphor layer. With a typical layer thickness of about 0.3 mm () they can be used for digital radiography of concrete. The required exposure time is comparable with the fluorescent screen-film systems. For better image quality higher exposure time is recommended.

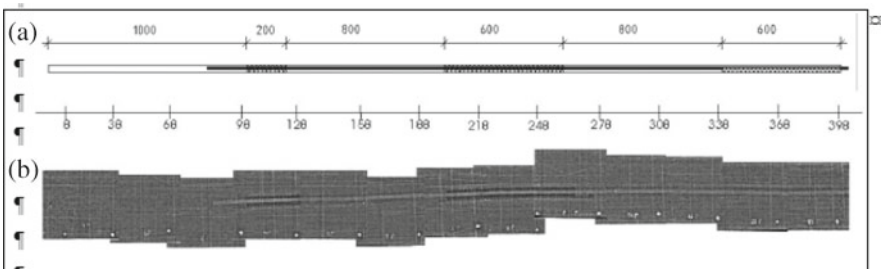

Fig. 6.3 Plan of tendon duct (diameter 40 mm) with artificial grouting faults (**a**) and verification with Gammagraphy with Cobalt 60 source (**b**); measured at Large Concrete Slab of BAM

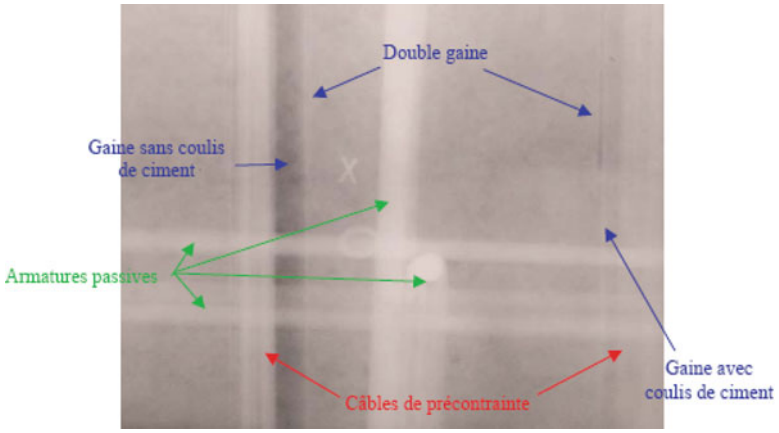

Fig. 6.4 Gammagraphy of bridge element with Cobalt 60 source

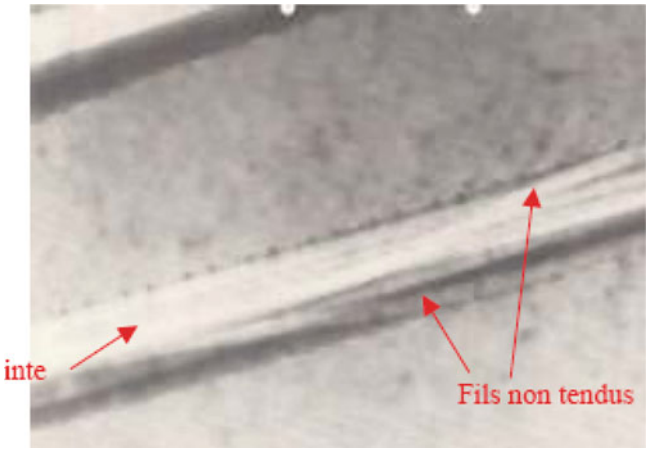

Fig. 6.5 Non prestressed strands imaged with Cobalt 60 source

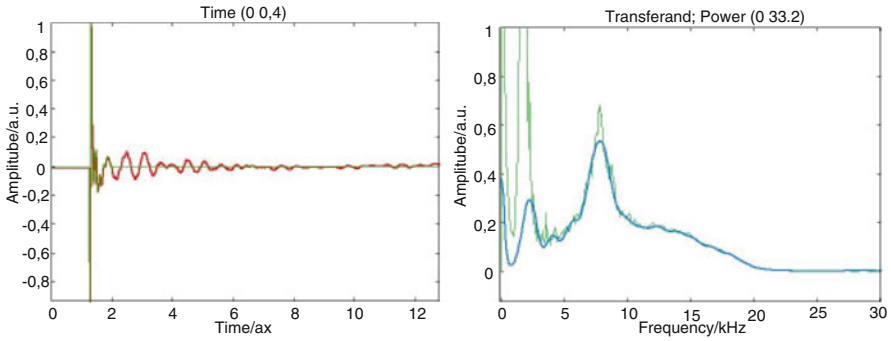

Fig. 6.6 Result of Impact-Echo point measurement for a specimen (thickness 0.25 m) containing tendon ducts (diameter 41 mm) [Algernon, 2007]

Of course it has to be stated out that radiographic techniques demand strict application of safety and radiation protection. This is regulated in the radiation protection ordinances in the different countries.

4 Echo Methods with mechanical waves: Impact Echo

The acoustic echo methods are divided in impact-echo and ultrasonic echo (see §5). Both can principally be used for point measurement. Equipment and evaluation software is available for this purpose furnished by different manufacturers. These methods are briefly described. Imaging methods are in the intermediate state between development and application. Several examples at specimens and post-tensioned concrete structures are described.

4.1 Application of the impact-echo method for tendon ducts

As described in Chapter 2 (§ 3), impact-echo is a mechanical wave method based on analysis of the multiple reflections after a mechanical impact and their evaluation in the frequency mode (Fast Fourier Transform, FFT).

An example measured at a concrete specimen containing grouted and ungrouted tendon ducts (diameter 41 mm) is depicted in Fig. 6.6.

Concerning the assessment of this method for tendon ducts opinions slightly differ. The method was standardised in USA in 1986 and there are manufacturers and publications who certify a good reliability for localizing grouting faults in tendon ducts by point evaluation [Sansalone and Streett, 1997], [Lin and Lin, 1997]. Other authors deduced after thorough studies that this is only possible applying imaging evaluation [Lausch et al, 2002], [Groβe et al, 2007]. One of the reasons is appearance of disturbing effects caused by geometry. In recent years applications working with point evaluation for tendon ducts presented at international conferences became

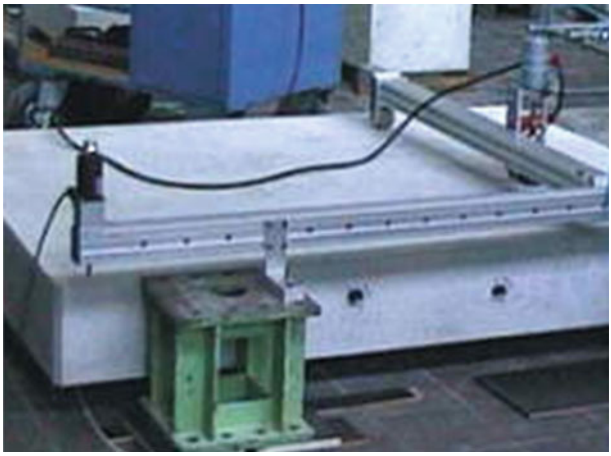

Fig. 6.7 Automated pneumatic scanning device with IE applied on a test specimen (after [Lausch et al, 2002])

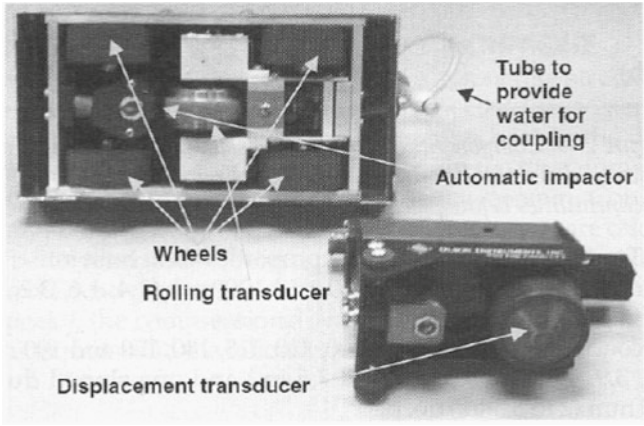

Fig. 6.8 Impact Echo scanning device with rolling transducer (after [Tinkey et al, 2005])

irrelevant, whereas imaging results were presented numerously [Wiggenhauser and Schickert, 2003], [Al Qadi and Washer, 2006].

There are impressive results for measurement and evaluation of large building elements with imaging impact echo ([Tinkey et al, 2005], [Abraham and Cote, 2002], [Colla et al, 1999], [Maierhofer et al, 2004]). Two examples of scanning devices are depicted in Figs. 6.7 and 6.8. The first is an application of impact-echo system mounted on an automated pneumatic scanning system, the second is an impact echo scanning device with a rolling transducer assembly incorporating multiple sensors.

Also microphones are applied for non-contact measurement [Zhu and Popovics, 2007]. Some examples are cited in the next sections. Laser interferometers are also under study for they have the advantage of being very large frequency band sensors

([Abraham et al, 2009], [Abraham and Popovics, 2010]). Their main disadvantage is that they often require surface preparation.

Another approach of evaluating Impact Echo data is in discussion since several years. It is based on the assumption of higher frequency modes after impact excitation. It is named Stack Imaging of Spectral Amplitudes Based on Impact-Echo (SIBIE [Ata et al, 2007]). Research results are briefly described in § 4.4.

There are different approaches to explain the origin of multiple reflections after mechanical impact in concrete. The easiest explanation is the appearances of resonant multiple reflections at a plane reflector, which are analysed by Fourier transform techniques. But this method needs correction factors for different geometrical shape of concrete elements [Sansalone and Streett, 1997].

[Gibson and Popovics, 2005] have analyzed the multiple reflections after impact excitation as guided waves (Lamb waves). In slab like components the resonant wave is explained as a resonance of the mode S_1 of a symmetric Lamb wave. Thus the calibration factor (ß=0.96) as introduced by [Sansalone and Streett, 1997] for the resonance frequency of slabs is not necessary.

In the simplest way the wave velocity can be measured from at a point of known thickness of the slab. When it is not possible, the velocity must be measured at cores, for example. Since they have a differing geometry, other wave modes can occur (e.g. dilatational waves) and conversion factors must be applied. These factors depend on Poisson ratio. For surface waves other effects have to be considered. This has less importance for localizing grouting faults, thus these aspects are not discussed in detail in this overview.

The criteria for distinguishing between grouted and ungrouted tendon ducts are described differently in the literature. There are two main criteria:

1. Change in the multiple reflection frequency between concrete/air and concrete/steel interfaces (quotient 4 instead of quotient 2 in Eq. 1)
2. Shift of the back wall echo frequency to lower frequency when the duct is ungrouted.

Short comment on criterion 1:

This is the most frequent criterion applied for impact echo point measurement. In [Sansalone and Streett, 1997] it is described as switch between pressure waves and tension waves depending on the type of reflecting interface (concrete/air or concrete/steel, respectively). It theoretically reduces the impact-echo frequency to one half. Another approach of explanation is the sign of the reflection coefficient, which switches from positive (concrete/steel) to negative (concrete/air) (phase jump). Recent experimental and theoretical considerations show that the frequency shift is much smaller as suggested for typical tendon duct diameters [Schubert and Köhler, 2008].

Imaging impact echo works mainly with criterion 2.

Short comment on criterion 2:

For the effect that the back wall frequency is shifted to lower frequencies (indicating larger thickness) the influence is twofold. The basic explanation considers the ray

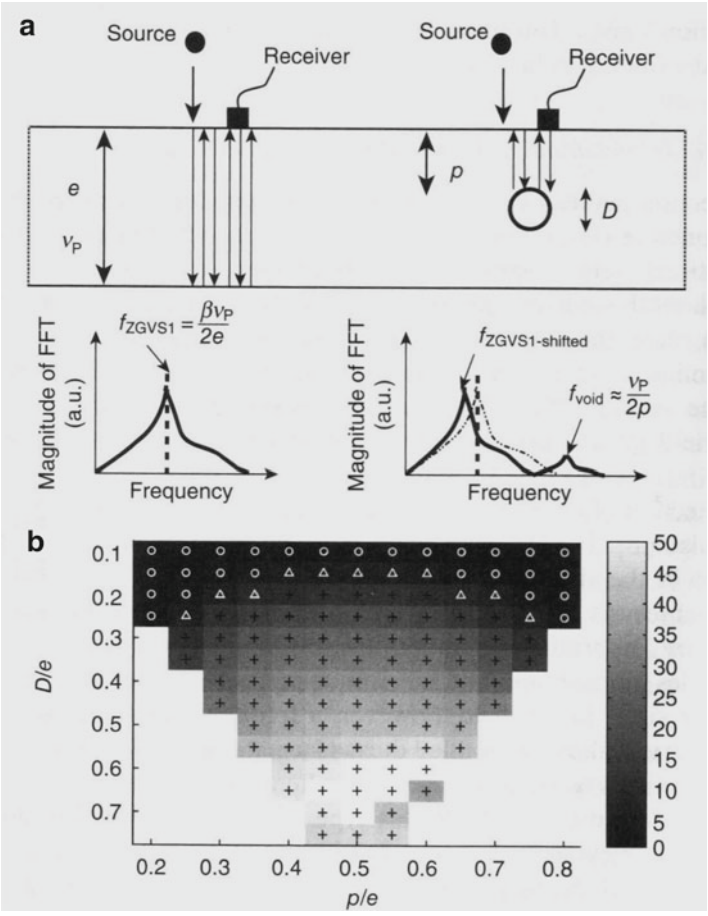

Fig. 6.9 (**a**) Schematic diagram of the impact-echo method for the detection of a small-sized void (**b**) Finite element evaluation of the thickness resonance frequency shift, in percent, above a void [Abraham and Popovics, 2010]

path of the longitudinal waves: in case of a void, the ray path becomes larger, which means a higher frequency of the multiple reflections.

Voids in concrete, especially in tendon ducts are reflectors for elastic waves, but they also reduce the concrete strength in their vicinity. This has the consequence that the elastic constant and the vibration frequency are changed in relation to the position of the void relative to the centre of the concrete slab. Following this argumentation the shift of the back wall echo caused by a void depends on the concrete cover of the tendon ducts [Lausch et al, 2002]. Experimental results of that shift are presented in § 4.3 (impact echo imaging).

There are thorough theoretical considerations, which consider both effects [Roenelle and Abraham, 2006]. In Fig. 6.9, the principle of the frequency shifted by the presence of a voided tendon duct is demonstrated. Here ZGVS1 indicates the

Zero Group Velocity of the Symmetric mode of a lamb wave. The thickness resonance frequency is shifted towards lower frequency caused by the void (diameter D). The lower part of the Fig. 6.9(b) shows the result of a finite element evaluation of the frequency shift in dependence of the diameter D and concrete cover p of the void [Abraham and Popovics, 2010].

4.2 Point and Linear Measurement and evaluation

In reality the impact echo signal often is superimposed by disturbing signals caused by geometry. Additionally impact echo theory only works properly for plane reflectors. Cylindrical targets as tendon ducts and even unstructured targets as honeycombing can lead to different behaviour of multiple reflections. The clearness of the signals mainly depends on the ratio between depth and diameter of the target. Following [Sansalone and Streett, 1997], ducts can be measured until a ratio of 3, other authors describe the difficulties, but they don't consider it as realistic to deduce an exact limit ([Lausch et al, 2002], [Groβe et al, 2007]).

In the Advice Notes from UK [Forde, 2006] a special carefulness is proposed, when the reflection objects are cylindrical like metal ducts. After this the advice is a need to pay attention to the input frequencies and the consequential wavelength in relation to the duct diameter. The proposed impact echo frequency runs from a minimum frequency of 19 kHz excited with an impactor diameter of 15 mm to a maximum frequency of 69 kHz excited with impactor diameter of 4 mm. In the first case the minimum target diameter is 105 mm (λ) and the depth range runs from 105 mm to 840 mm. In the latter case the minimum target diameter is 58 mm (λ) and the depth range runs from 29 mm 232 mm.

Figure 6.10a) shows the frequency response from a voided duct whilst Fig. 6.10b) shows the frequency response from a fully grouted duct. These results were taken at the middle of a concrete beam to reduce any border effects. It can be seen that from Fig. 6.8 the initial peak (fT) has moved forward from 4.9 (plain concrete), and there is a peak with a higher frequency, these being typical of a voided duct. In Fig. 6.8 the initial fT has not moved forward and there is a frequency peak at 6 kHz [Forde, 2006].

The difficulties to read proper impact echo results in point measurement was one of the reasons to develop the impact-echo imaging possibilities described in the following § 4.3.

4.3 Impact-Echo imaging

In applying point-measuring methods in a way that several data points are collected along a line, imaging techniques can be used. This method is improved into a scanning test method to visualize test results as an Impact-Echogram, similar to a B-scan in ultrasonic pulse echo or a GPR radargram. The amplitude of the

Fig. 6.10a) Result of an impact-echo test over an ungrouted (voided) tendon duct

Fig. 6.10b) Result of impact-echo test over a grouted tendon duct [Forde, 2006]

frequency power spectrum is displayed colour coded or in greyscale over the position of the measurements and frequency like shown in Fig. 6.11 ([Colla et al, 1999], [Groβe et al, 2007]).

With automated testing in dense measurement grids Impact-Echo measurements can image very detailed the thickness of a concrete slab. When scanning is extended to a 2-dimensional grid, IE-results can be shown as 3-D images as shown in Fig. 6.12.

Usually impact-echo imaging of ducts works indirectly. This is demonstrated in Fig. 6.13a)-b), where the shift of the resonance frequency of the back wall signal is clearly visible. As mentioned above, several effects influence the shift of the back

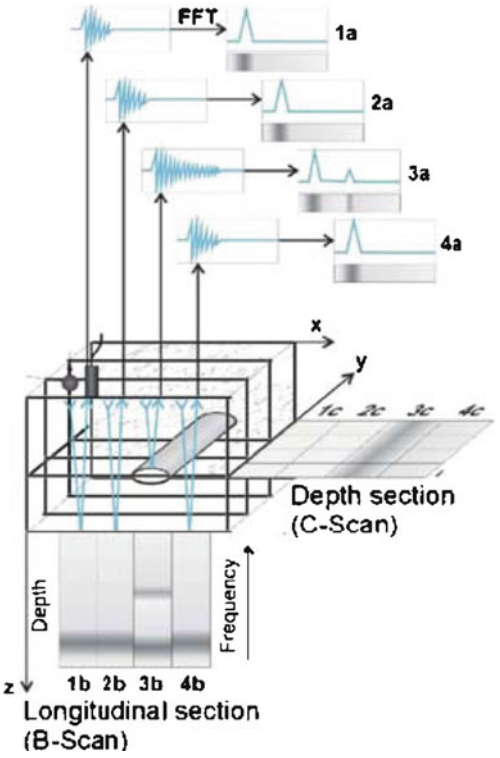

Fig. 6.11 Principle of Impact-echo imaging (Layout: D. Schaurich)

wall echo: diameter, grouting condition, stiffness, concrete cover, position in the concrete slab ([Lausch et al, 2002], [Wiggenhauser, 2003], [Groβe et al, 2007]).

In a systematic study at a test specimen under laboratory condition it was shown that ungrouted and grouted areas can be indicated by impact echo imaging. This is demonstrated in Fig. 6.14. The built in grouting faults are depicted in part a) of the Fig. Part b) shows the impact-echo B-scan. The different shift of the back wall resonance below the duct is clearly visible. Apparently regions having a stronger shift correspond to voids in the tendon duct. Regarding the impact-echo c-scan in part c) of Fig. 6.14, the ungrouted areas are imaged in the correspondent depth section ([Maierhofer et al, 2004], [Wiggenhauser et al, 2007]).

Another approach to measure and image the shift of the back wall echo is to use a a laser interferometer as receiver. It was realized at a test slab, which is 0.25 m thick and includes various tendon ducts - filled and empty - together with an empty thick steel pipe. The source is maintained at a fixed distance from the wall with a wheel so that the impact is reproducible. The presence of empty tendon duct are clearly seen on the C-SCAN at a frequency nearby the impact-echo thickness resonance frequency ([Abraham et al, 2010], [Abraham et al, 2010]).

Experimental studies about indicating voids by the shift of back wall echo also were also performed applying the impact echo scanner described above (see Fig. 6.8). An example is shown in Fig. 6.15. It demonstrates that the back wall echo show a smaller increase of apparent thickness over a well-grouted steel duct and a more significant

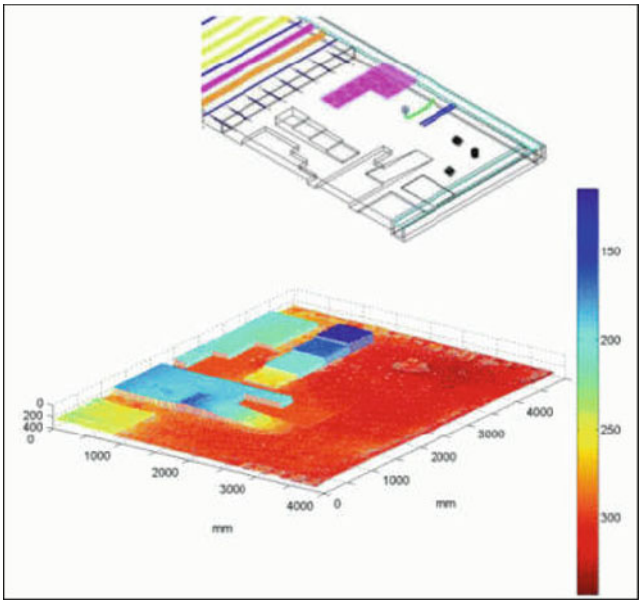

Fig. 6.12 Imaging of IE results of the Large Concrete Slab at BAM, Berlin

Fig. 6.13a) Impact echogram of concrete specimen with tendon ducts (grouted and ungrouted without strands)

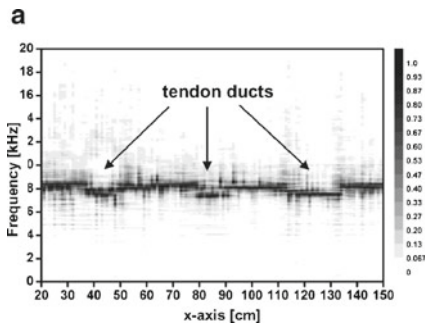

Fig. 6.13b) Specimen with three tendon ducts, different concrete cover and grouting condition (after ([Lausch et al, 2002])

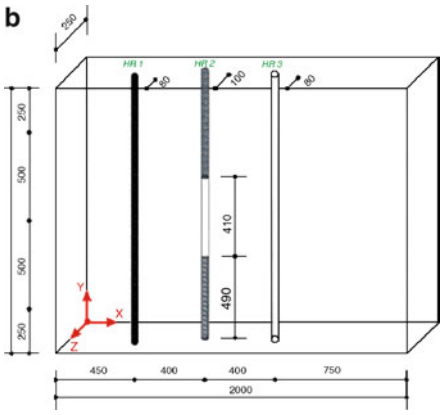

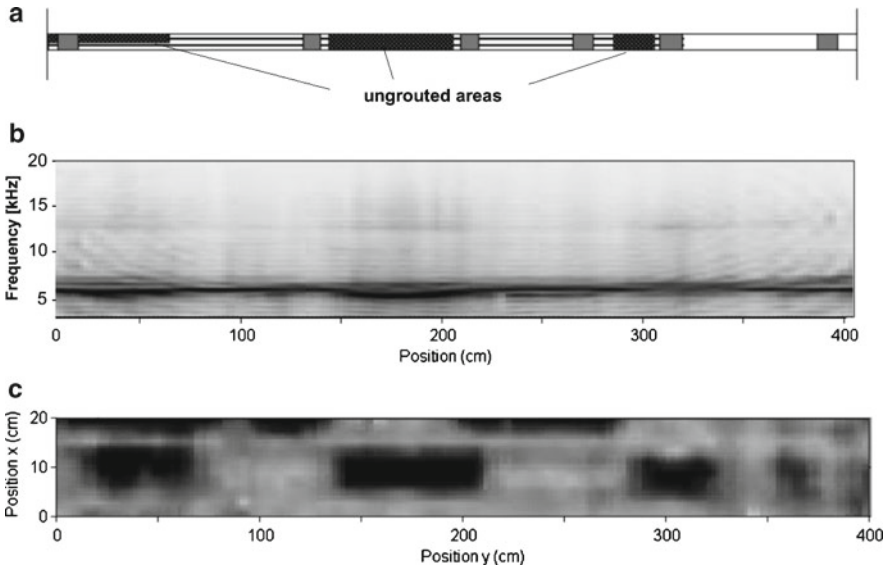

Fig. 6.14 Impact echo imaging of tendon duct with artificial voids: **a**) plan, **b**) Impact echogramm (longitudinal section above duct, B-scan; backwall echo 6.16 kHz, shifted backwall echo around ducts., **c**) Depth section for shifted backwall echo (5.63 kHz) (after [Groβe et al, 2007])

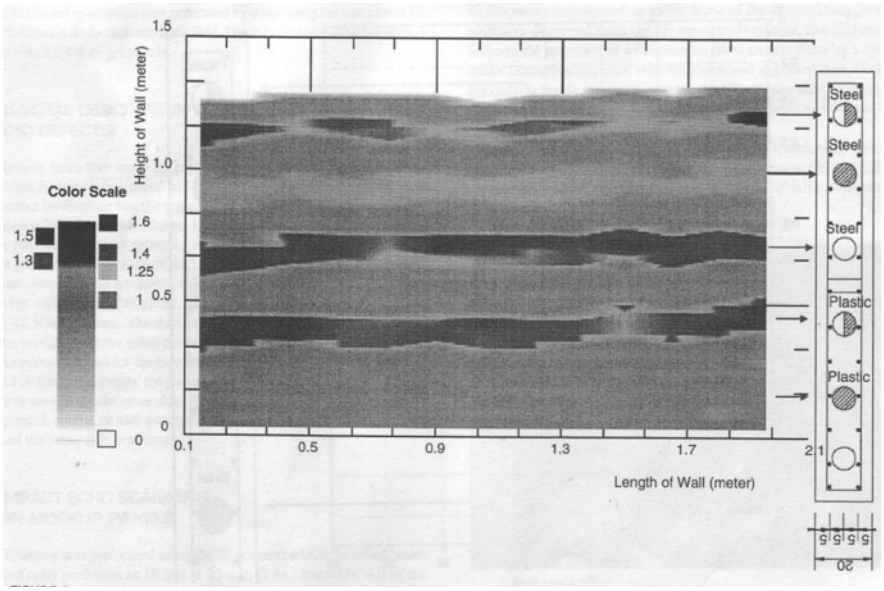

Fig. 6.15 Result of impact echo scanning experiment of a specimen with a thickness of 0.2 m. Visualisation of actual thickness indicated corresponding to the colour scale [Tinkey and Olson, 2008]

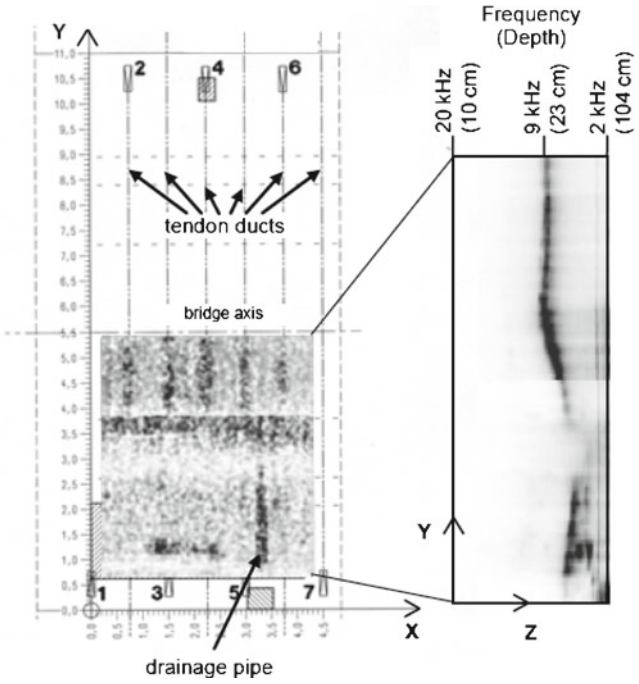

Fig. 6.16 Results of impact-echo-measurements on a bridge deck; left: C-scan parallel to the measurement surface at 8.6 kHz, right: projection of all B-scans parallel to the y-axis

increase of apparent thickness over empty and partially grouted ducts [Tinkey and Olson, 2008]. These experiments were carried out on tendons without strands.

Examples from application at bridges

On-site investigations with impact-echo at concrete structures up to a thickness of 83 cm show, that the back wall of these concrete structures could be reliably detected. The localization of tendon ducts and the assessment of the grouting conditions at the tendon ducts of the bridges are often difficult. As shown at the example of results in Fig. 6.16 the lateral position of tendon ducts could be determined by a displacement of the reflection from the backside of structure during on-site performances.

In Fig. 6.16, two images of an impact echo data set are shown as results of measurements on a deck of a box girder bridge. On the right side a B-scan projection is presented. The backside, which is partially not parallel to the surface, is clearly visible at a frequency of approximately 9 kHz. This frequency is equivalent to the thickness in the middle of the deck (approx. 24 cm). On the left side of this figure a C-scan (slice parallel to the surface) in the depth of the backside is shown. The lateral positions of the tendon ducts are clearly visible from y = 3.7 m to y = 5.4 m as displacements of the backside reflection. A drainage pipe causes high intensity between the tendon ducts nos. 5 and 6. At these measurements the distance between the top of the deck that means the measurement surface and the tendons was not determinable. Otherwise the concrete cover of the tendons could be determined carrying

out measurements on the bottom side of the deck. Here, wave reflections from the tendons were directly detected as well [Wiggenhauser et al, 2007].

4.4 Interpretation and research: the SIBIE procedure

For a better evaluation of impact-echo data and in order to improve the method, an imaging technique has been applied to the data in the frequency domain. This procedure is named SIBIE (*Stack Imaging of Spectral Amplitudes Based on Impact-Echo*) [Ohtsu and Watanabe, 2002]. SIBIE procedure is an improved alternative method to interpret impact echo data. It is an imaging technique applied to the impact-echo data in frequency domain.

In the procedure, first, a cross-section of concrete is divided into square elements. Then, resonance frequencies due to reflections at each element are computed. The travel distance from the input location to the output through the element is calculated for each square element.

Following the developers of the method, there are two resonance frequencies due to reflections at each element are calculated:

$$f'_2 = C_p / r_2 \text{ and } f_R = C_p / R$$

where C_p is the velocity of P-wave, r_2 is the distance between an element and the output location, R is the total travel distance. Spectral amplitudes corresponding to these two resonance frequencies in the frequency spectrum are summed up at each mesh. Thus, reflection intensity is estimated as a stack image at each element. The minimum size of the square mesh Δ for the SIBIE analysis should be approximately equal to $C_p \, \Delta t/2$, where Δt is the sampling time of a recorded wave.

Following the authors, SIBIE has been successfully applied to void detection within tendon ducts as well as surface-crack depth identification ([Ata et al., 2007], [Alver and Ohtsu, 2007], [Alver et al, 2004]). In these papers results on locations of voids and depths of surface-cracks identified by SIBIE are described. One example of the method is described below, following citation [Alver and Ohtsu, 2006]. It is the result of application of impact-echo method and SIBIE procedure to a concrete specimen with a metal-duct, presented in Fig. 6.17. The frequency spectrum obtained by an impact-test of the specimen is shown in Fig. 6.17a). The resonance frequency of the void f_{void} is indicated with an arrow and is assigned as close to the calculated value [$f_{void}=C_p/2d$], as possible. SIBIE analysis was carried out by using a frequency spectrum shown in Fig. 6.17a) and a result is shown in Fig. 6.17b). Black colour of the high reflection zones is clearly observed in front of the void. Following the authors in this way it is demonstrated that SIBIE is able to identify such voids within tendon-ducts.

During several discussions on conferences, the presenters of SIBIE-results were asked to prove the existence of two resonance frequencies additionally for large concrete specimens in order not to avoid confusion resonances with geometrically caused multiple reflections and oscillations of the specimen. This should be especially important in case of cracks, because following the usual Impact Echo theory there are no multiple reflections between measuring surface and crack tip.

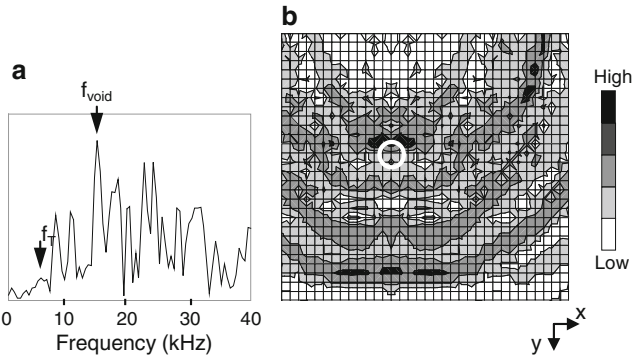

Fig. 6.17 **a**) Frequency response and **b)** SIBIE result by impact test of a concrete specimen with metal duct

5 Echo Methods with mechanical waves: Ultrasonic Echo

The mechanical wave methods are divided in impact-echo (see §4) and ultrasonic echo and ultrasonic through transmission, that will be presented in §5 and §6. Both can be used for point measurement. Equipment and evaluation software is available for this purpose furnished by different manufacturers. These methods are briefly described.

Since about 1995 imaging and reconstruction methods are developed for measuring data, which are taken in a line or a measuring mesh (2D data acquisition). For both Impact-Echo and ultrasonic echo methods, large progress was achieved; examples are summarized in this text.

5.1 Introduction, principle

The frequency range for ultrasonic echo measurement in concrete elements leads from 20 kHz to 200 kHz. Pressure-waves (longitudinal waves) as well as shear waves (transverse waves) are applied. For basics about ultrasonic low frequency echo methods for reinforced concrete see e.g. [Schickert and Krause, 2010].

From the research work of the last 15 years it can be followed that there are two criteria for localizing grouting faults in tendon ducts:

1. In the magnitude representation air inclusions show significant higher reflection intensity (total reflection) than for grouted steel rebar or strands. This criterion follows from the different reflection coefficients of the interface concrete/air and concrete/steel as is applied since 1995 ([Krause et al, 1997], [Jansohn et al, 2002], [Krause et al, 2003], [Schickert, 2005].).
2. In imaging the phase value or signal shape of the reflected signal the distinction between air filled areas and grouted steel bars or strands is realized by the phase difference of 180°. This criterion considers the phase difference between the reflections at the interface concrete/air (material with smaller acoustic impedance)

relative to the reflection concrete/steel (larger acoustic impedance). It recently was redeveloped applied as a part of acoustical imaging [Mayer et al, 2008 and 2008b]. Up to now this criterion is only developed for few types of tendon ducts. The systematic automated application and research on site conditions are subjects of actual research and development project [Krause et al, 2011].

A third effect is known from several measuring results at tendon ducts: in several cases reflecting signals are appearing in the SAFT-B-scans (*Synthetic Aperture Focusing Technique*) corresponding to the depth of the bottom side of the tendon duct. In completely voided areas the reflection happens always at the topside of the duct (smallest concrete cover relative to the measuring surface) [Krause et al, 2011]).

Especially in older post-tensioned structures it may happen that the duct is correctly grouted but the mortar was shrinking during hardening and will cause minor delaminations between duct and grouting mortar. This means that such a duct would show the same ultrasonic reflection properties than a completely voided duct. Experiences with opened ducts show that the shrinking process is not always uniform. For example light rust films may partially cause bonding beween duct and grouting mortar. However it should be noted that high ultrasonic back scatter intensity of ducts does not inevitably indicate poor grouting conditions. Up to now the main aim of the method is to indicate suspicious areas. For the final assessment minor destructive opening of the tendon ducts seems useful.

5.2 *Ultrasonic Point Measurement and evaluation*

Tendon ducts can clearly be recognised as reflectors in single reflection curves. This follows from the fact that reflection coefficients at steel tendons as well as at air inclusions have large values (R_{steel} = 60% and R_{air} = 100%; idealized for plan and thick reflectors). Since modern ultrasonic echo equipment is capable to measure back wall reflections in concrete for up to 0.5 m or 1.50 m depending on the site conditions, tendon ducts having a diameter of 40 mm or more result in a clear echo, when they have typical concrete covers between 50 mm and 150 mm. Of course the position of the probes has to be directly above the duct and the wave propagation must not be shielded by reinforcing bars.

One example of indicating an artificial compaction fault around a duct is presented in Fig. 6.18. P-wave transducers were applied in T/R mode (transmitter and receiver separated but close together [Taffe et al, 2008].

5.3 *Linear Measurement and 2D representation of the data*

When several measuring points are combined to a measuring line, the results are normally represented in a cross section or longitudinal section (also called ultrasonic B-scan), respectively. In this B-scans the magnitude of the reflection is represented

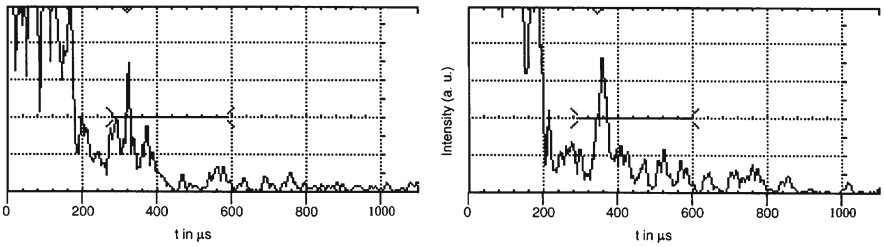

Fig. 6.18 Ultrasonic pulse echo with interpretation of ultrasonic echo time curve (A-scan) measured above a compaction fault, hence the concrete cover is reduced (left); right: reflection at steel

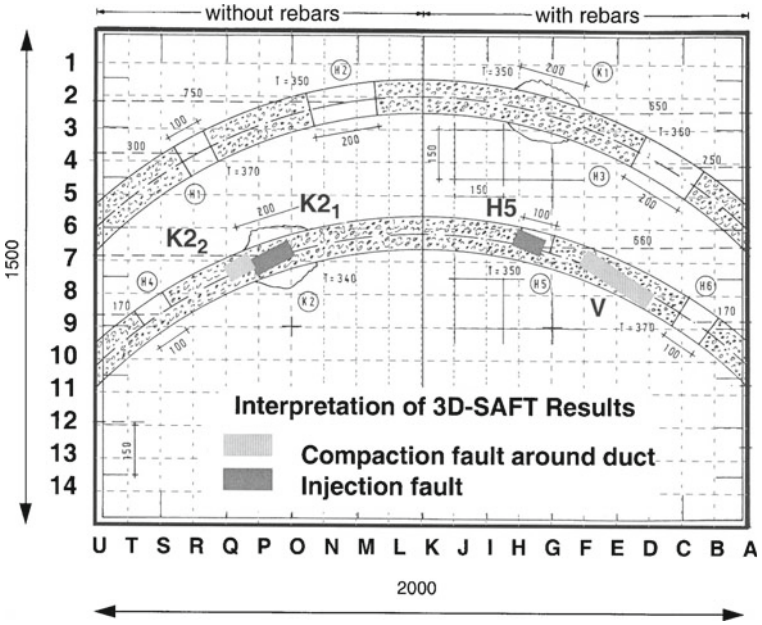

Fig. 6.19 Interpretation of results obtained with ultrasonic imaging (experiments for lower duct)

in grey values or false colours. From this low and high reflecting areas can be indicated [Krause et al, 1997].

Application of shear wave dry contact equipment enables measuring above tendon ducts and representing their reflecting magnitude. There are results successfully assigned to ungrouted areas in tendon ducts [Kroggel et al, 2002]. The reflection magnitude gives hints for compaction faults around and grouting faults in tendon ducts (specimen sketch see Fig. 6.19, upper duct).

These results were obtained in a round robin test at BAST (Federal Highway Institute) at two specimens with artificial voids and different amount of non prestressed reinforcing bars [Krause et al, 2002]. In this double blind tests also ultrasonic imaging methods were applied, which partly indicated voids in tendon ducts.

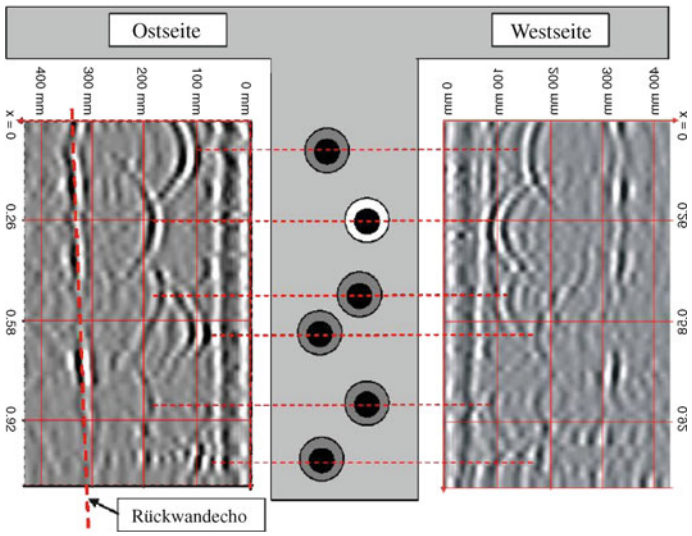

Fig. 6.20 Reflection signals from a grouted and ungrouted area of a tendon duct in a prefabricated road bridge (diameter 80 mm concrete cover: 100 mm to 200 mm [Sodeikat and Dauberschmidt, 2008]

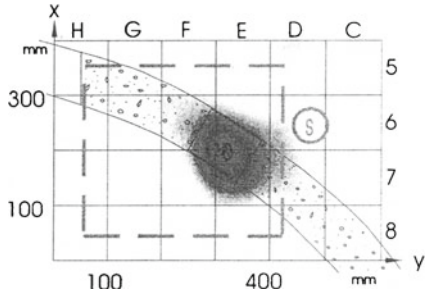

Fig. 6.21 Imaging of void in tendon duct with Laser interferometer and reconstruction calculation

These experiments were carried applying a laser interferometer as ultrasonic receiver (see §5.4.1., Fig. 6.21).

Analysing the pulse shape and estimating and the value of the reflected pulse in ultrasonic B-scans is rarely possible in practical application. The signal from of the reflecting pulse is overlaid by backscatter effects of concrete (structural noise) so that the phase jump between two different locations of the probe normally is not visible clearly enough for a reliable assessment of grouting condition. One example is depicted in Fig. 6.22.

It is an example measured at a prefabricated road bridge in Germany applying the equipment mentioned above with actual evaluation software being able to switch between raw data (HF signal) and rectified data [Sodeikat and Dauberschmidt, 2008] (see Fig. 6.20).

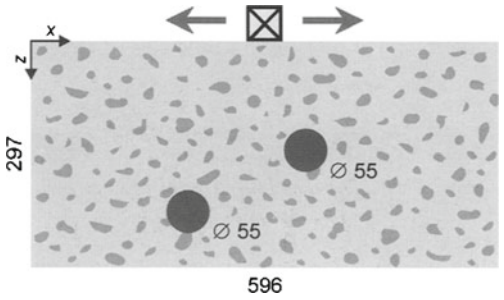

Fig. 6.22 Sectional view of the two-hole test specimen (dimensions in mm) [Schickert 2005]

5.4 Linear and 2D Measurement followed by Imaging with Reconstruction calculation (magnitude evaluation)

5.4.1 Examples in the laboratory

The examples described in the two previous sections are limited to few applications. The most impressive success in the last years was achieved applying linear and 2D measurements with successive imaging. This imaging is performed using reconstruction calculation with SAFT-Synthetic Aperture Focusing Technique. Here 2D and 3D applications in the heuristic time shifting approach [Schickert et al, 2003] as well as with Fast Fourier transform [Mayer et al, 2008] are applied.

The first example of 3D imaging of a void in a tendon duct was presented in 1996 in the frame of a round robin test carried out at a test specimen with artificial grouting faults in a tendon duct without strands [Krause et al, 1997]. The example depicted Fig. 6.21 was measured applying a broadband pressure wave pulse (f = 85 kHz) and a 2D scanning laser interferometer as receiver. For good signal/noise ratio retro reflecting colour was used.

The capability for imaging holes with linear measuring and 2D-reconstruction is demonstrated in Figs. 6.22 and 6.23. Applying broadband transducers excitation with rectangular pulses are guided along the known position of a tendon duct, and the data are registered with high repetition frequency. Applying a commercial equipment development together with statistical analyzing methods the localization of air inclusions is possible [Schickert 2005]. Figures 6.22 and 6.23 presents a result obtained at a borehole, which is partially filled with cement. Applying statistical evaluation a noise threshold is defined. Then the reflection magnitude indicates the filling degree of the duct.

The intensity criterion (No.1 in §5.1) is applied with shear waves and pressure waves. For both automated scanning systems are available. For shear waves dry contact transducers described above are applied. They are mounted in large scanners, which can measure surfaces up to 40 m^2 non-stop, because they don't need any

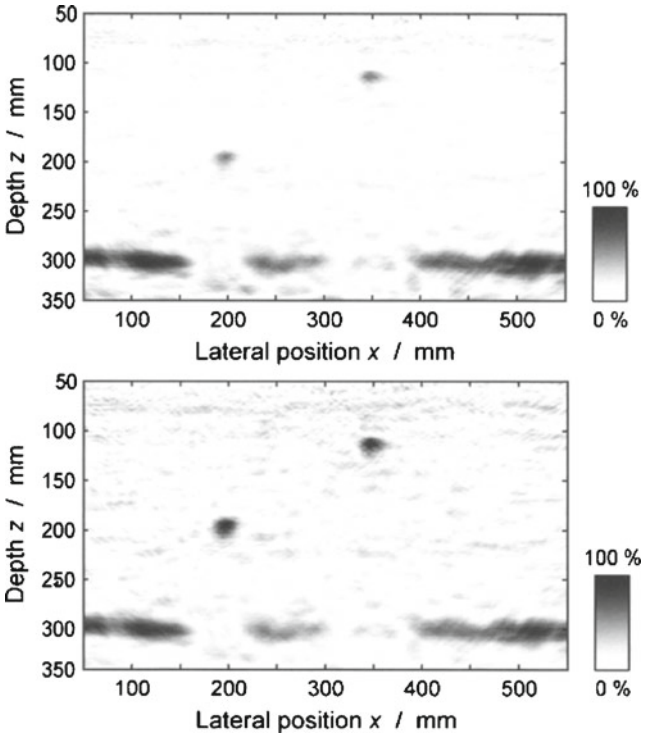

Fig. 6.23 SAFT reconstructions, depth corrected using reference reflectors (top) and noise statistics (down) [Schickert 2005]

coupling agent (Fig. 6.24). For automated measuring the p-wave transducers were coupled by water (Fig. 6.25). Another possibility for fast ultrasonic echo measurement is described in § 5.6.

Comparative tests were performed in the frame of the research group FOR 384. Figure 6.26 presents a test specimen with 80 mm tendon ducts containing 12 reinforcing wires (diameter 12 mm; side view Fig. 6.27a).

Figures 6.27a) and 6.28 show the experimental results for ultrasonic measurement and SAFT-reconstruction. In Fig. 6.27a) the shear wave measurements (ultrasonic frequency 55 kHz) are presented with 3D-SAFT reconstruction imaging ([Krause et al, 2003], [Krause et al, 2006]). In this case a longitudinal section parallel to the duct is presented (ultrasonic SAFT B-scan parallel x). In Fig. 6.28 the results of linear SAFT reconstruction of p-wave measurement are depicted (centre frequency 200 kHz of transmitting pulse). The jump in ultrasonic reflection magnitude appears at x = 800 mm in both measuring curves and corresponds to the change of grouting conditions.

A second feature in Fig. 6.27a) corresponds to the depth of reflecting signals from the interior of tendon ducts (criterion #2 described in §5.1). As can be seen in

Fig. 6.24 2D scanner working with linear drives and a pneumatic system to press the point contact transducers without coupling agent (at BAM Berlin)

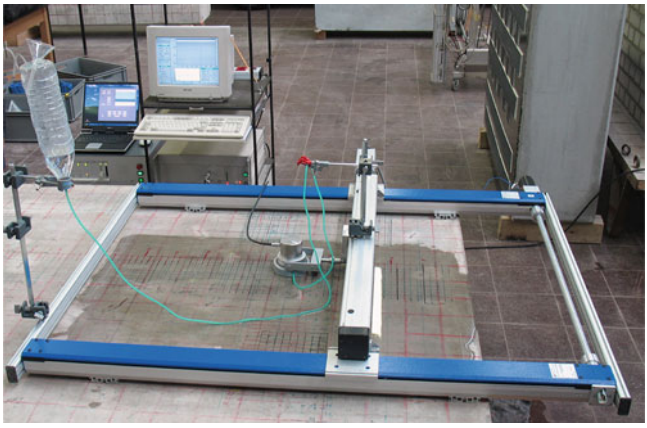

Fig. 6.25 Ultrasonic measuring head for pressure waves mounted in a 2D scanner working in pulse echo mode with water coupling (at MFPA Weimar)

Fig. 6.27b), the tendon duct has an air inclusion at the bottom side, which arrived unintentionally during the grouting process, being bedded on the opposite side (see photograph in Fig. 6.27b). The reflection line at z = 380 mm is obviously related to the existence of the air inclusion, but the measured depth doesn't exactly correspond to a direct reflection at the air inclusion.

The effect of a second signal for well grouted ducts measured with shear waves was also observed in practical applications at post tensioned concrete bridges [Krause et al, 2011]. The effect is not yet completely understood. It depends on the way, how the ultrasonic waves pass the grouting mortar and steel wires and/or propagate along the interface around the tendon duct (concrete/steel sheet/grouting mortar). An explanation

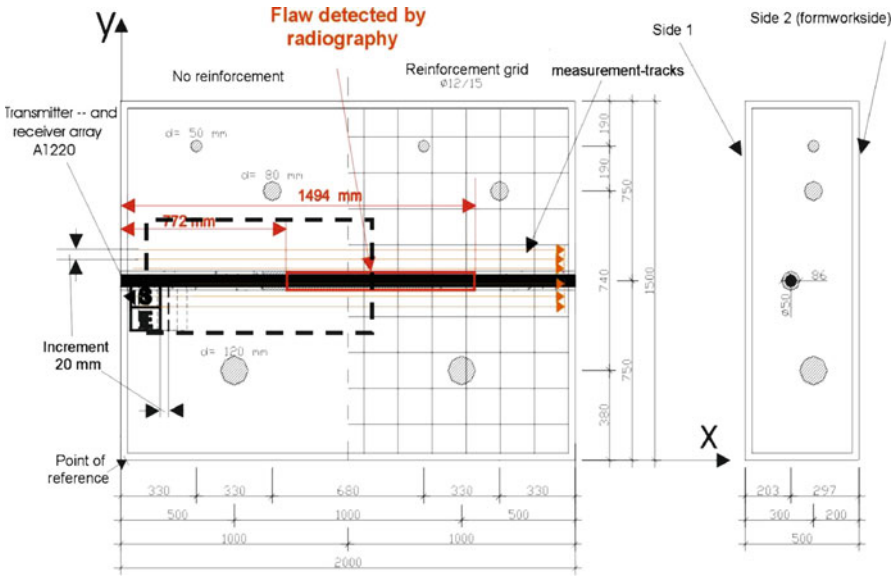

Fig. 6.26 Construction plan of test specimen BAM.NB.FBS.1, containing artificial voids in a tendon duct and styrodur balls. The location of the void in the duct was localized using γ-radiography. Rectangle: Area of pressure wave measurement MFPA Weimar (Fig. 28); Arrows: area of presented shear wave measurement BAM (Fig. 27)

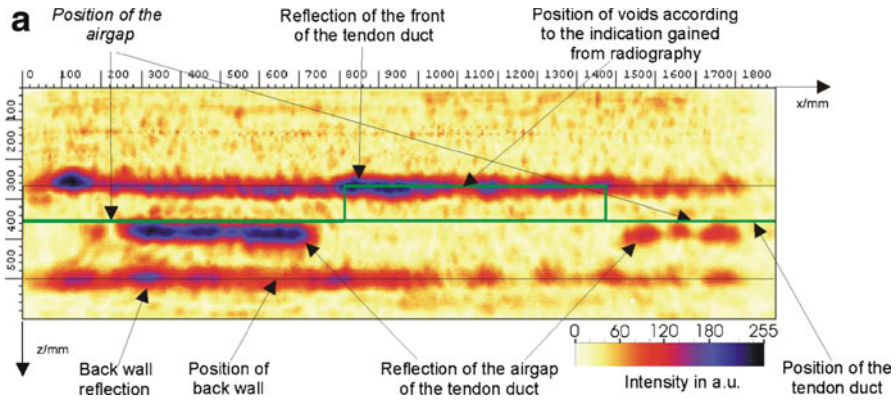

Fig. 6.27a) Result of imaging tendon duct in specimen FBS1with shear waves: B-scan above the tendon duct from 3D-SAFT reconstruction. Polarization axis parallel x

Fig. 6.27b) Side view of tendon duct on FBS1 (photograph)

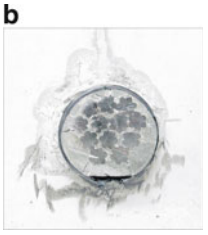

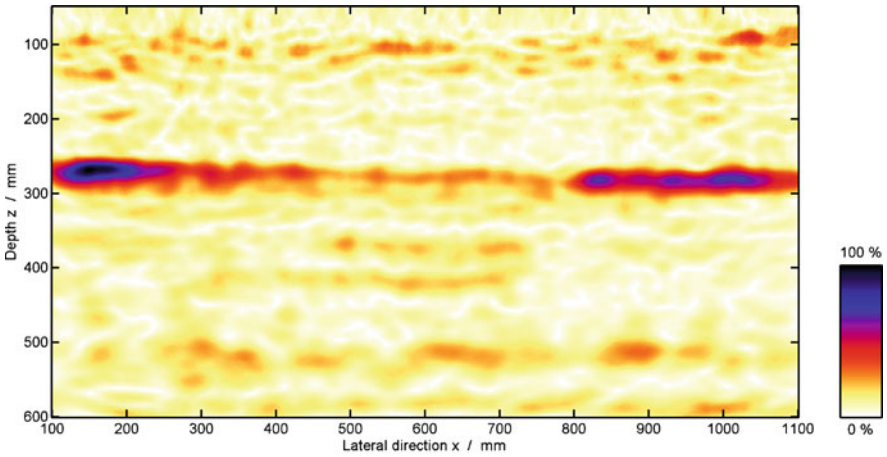

Fig. 6.28 Result of imaging tendon duct in specimen FBS1with pressure waves: B-scan above the tendon duct from 2D-SAFT reconstruction

with help of 3D modelling calculation including EFIT (*Elastodynamic Finite Integration Technique*) is still in the works [Krause et al, 2009].

5.4.2 Applications at post-tensioned concrete bridges

In order to assess and to improve the NDT methods for practical application, BAM together with partners regularly performs automated radar and ultrasonic-echo measurements on post-tensioned bridges. Investigations are carried out on areas on the inner and/or outer-side of webs and on the bottom and/or topside of decks with transverse pre-stressing (e.g. [Streicher et al, 2006], [Helmerich et al, 2008]). Those areas are marked with dark lines in a typical cross section (Fig. 6.29a). With exception of topside measurement, traffic on bridges is not affected by those activities.

Figure 6.29b) depicts an example of a large scale measurement of a tendon duct measured by means of scanning ultrasonic echo (shear waves 55 kHz) from the bottom side of the bridge. The duct is imaged in the depth range from z = 100 mm to 870 mm. Signals from the bottom side of the duct (close to ultrasonic probe) and partly from the area of the far side are recognisable. Further investigation of those effects is ongoing [Krause et al, 2011]. With ultrasonic 3D reconstruction (3D-SAFT) also tendons arranged behind others can be imaged. As an example Fig. 6.29c) presents from an investigated web.

5.5 Reconstruction calculation using phase evaluation

A qualitative distinction between steel and air reflections in concrete becomes possible, when the phase values of the ultrasonic signals are considered in the SAFT reconstruction calculation. This result was achieved within in the frame of the

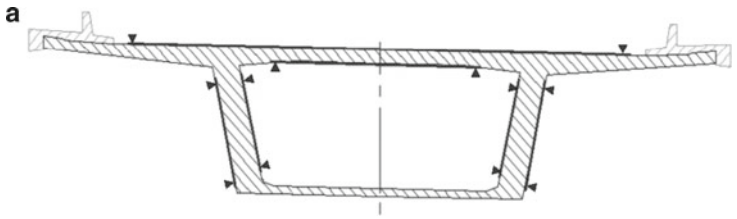

Fig. 6.29a) Investigated areas on box girder bridges using automated NDT-methods

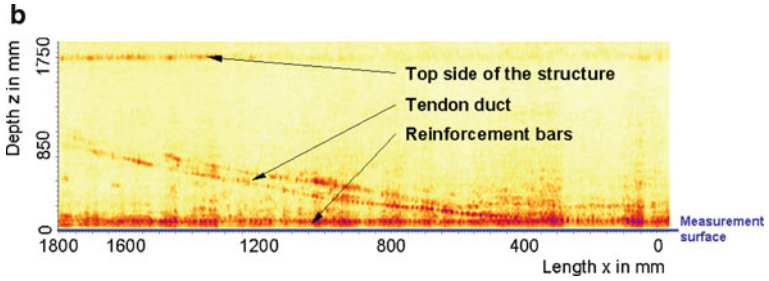

Fig. 6.29b) SAFT-B-projection of ultrasonic echo data, imaging the curvature of a tendon duct in the longitudinal section of a T-beam bridge [Streicher et al, 2006]

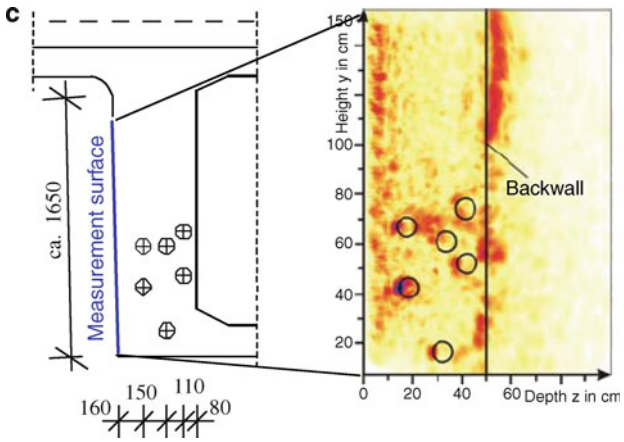

Fig. 6.29c) Arrangement of tendon ducts in the cross section of a box girder web, left: according to construction plan, right: located at a SAFT-B projection by ultrasonic echo [Wiggenhauser et al, 2007]

research group FOR 384 ([Mayer et al, 2006], [Patent, 2006]). A first study describes the method capability [Mayer et al, 2008]. In the following, two exam–ples are presented. The first was carried out at the Large Concrete Slab (LCS, see also Chapter 6, § 4.2.2), which was designed and constructed at BAM in order to realize typical

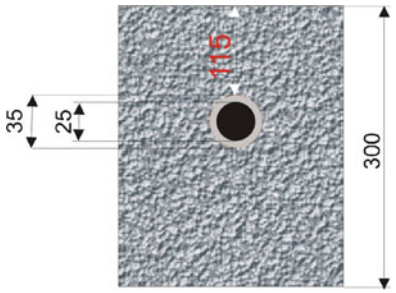

Fig. 6.30 Geometry and concrete cover for tendon D3 in LCS

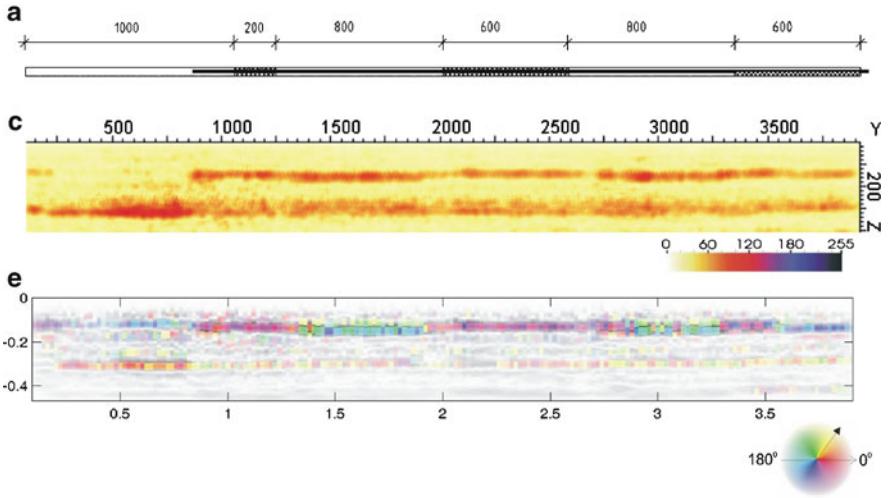

Fig. 6.31 Results for tendon duct D3 in LCL: **a)** Sketch of the specimen with desired grouting faults; **c)** Result of scanning with 55 kHz shear waves, polarization parallel to the ducts: magnitude representation in a B-scan of 3D-SAFT reconstruction; **e)** Phase values of reflecting pulses around the maximum of each reflector calculated from FT-SAFT reconstruction

testing tasks for the comparison of different NDT methods and their validation [Taffe et al, 2003].

One part of this concrete slab contains 11 tendon ducts in the diameter range from 40 mm to 120 mm having concrete cover between 80 mm and 200 mm with artificial grouting faults. The grouting was performed similar to industrial application (pressure grouting). The geometry of tendon D3 is depicted in Fig. 6.30. It has a concrete cover of 115 mm. It is a steel bar in a duct having a diameter of 35 mm. The experiments were carried out using a 55 kHz point contact transducer working with an automated scanner.

Figure 6.31 depicts the results of ultrasonic imaging experiments of the tendon D3 in comparison with the plan of artificial grouting faults (shaded in Fig. 6.31a)). Their location was verified applying γ-radiography. Figure 6.31c) depicts the magnitude

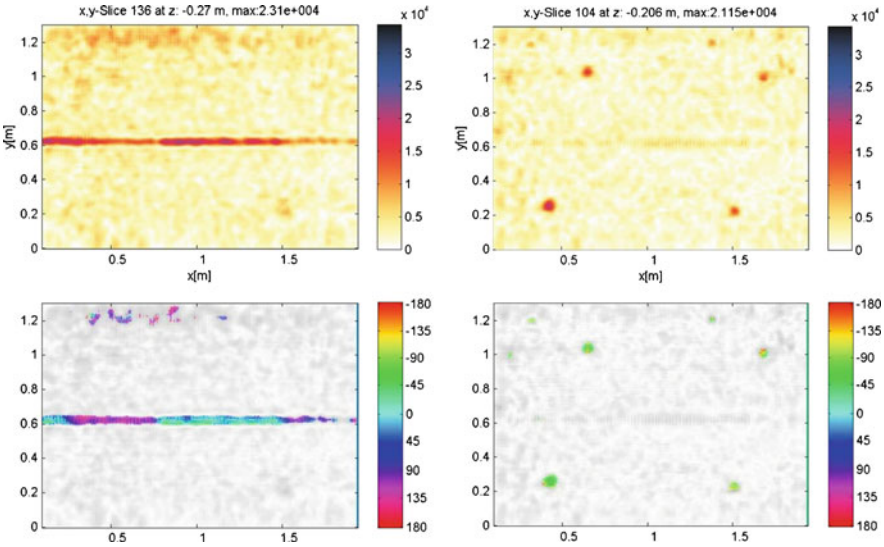

Fig. 6.32 Ultrasonic imaging of artificial grouting faults and styrodur balls by means of 3D-SAFT phase evaluation (depth sections (C-scans)) specimen FBS1, SAFT-B-scans of magnitude already shown in Fig. 6.27., see also plan Fig. 6.26. The upper parts of the figures show the magnitude and the lower part the phase value of the reflected pulse, respectively. Left: depth section of the top side of the tendon duct (z = 270 mm); Right: Depth section in the depth of styrodur balls (z = 206 mm). Significant phase value difference between reflection at air inclusions / styrodur and steel.

of ultrasonic reflection intensity as longitudinal section along the tendon duct (ultrasonic B-scan). There is no significant change in reflection intensity at ungrouted areas.

Otherwise the phase evaluation shown in Fig. 6.31e) shows a very clear difference between air filled and well grouted areas. The colour coded image indicates a shift of the phase value of 180º between grouted and ungrouted areas.

This means that the phase evaluation clearly indicated the difference between air filled and grouted areas, and allows distinguishing between reflection at air and reflection at steel. This is not possible from the intensity representation in this case.

The second example concerns the specimen containing artificial grouting faults and styrodur balls already presented and discussed in section 4.5.1 (Figs. 6.26 to 6.28). The phase evaluation demonstrates the capability to characterise even small air inclusions. Figure 6.32 shows the C-scan (depth section) in the depth corresponding to of the top side of the tendon duct (z = 270 mm), whereas Fig. 6.26 shows the plane of the styrodur balls (z = 206 mm). All balls in the diameter range from 120 mm to 30 mm are imaged. The phase difference between air inclusions (ϕ = 0 to 45°) and steel (ϕ = -130°) is significant.

Fig. 6.33a) Linear array with dry contact transducers

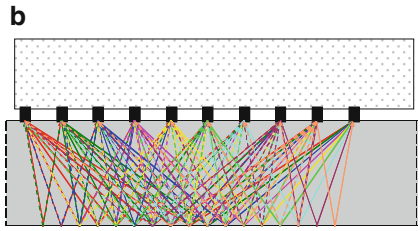

Fig. 6.33b) Principle of data acquisition

5.6 Ultrasonic Echo with Linear Array

In order to accelerate the ultrasonic data acquisition, a linear array was developed in co-operation between BAM and ACSYS ([Kozlov et al, 2006], [Krause et al, 2008]). It consists of 10 lines à 4 dry contact shear wave transducers working with 50 kHz. The distance of the lines is 35 mm in the present modification. The transducers and the electronics are mounted in a handheld box easily to be applied at concrete surfaces (Fig. 6.33a)). The ten lines are switched as a multistatic array, that means one line acts as transmitter and all others as receiver, then the second as transmitter, and so forth as shown in Fig. 6.33b). The data transfer is organized in the way that the whole data set is measured and stored in less than 1 second per location.

The data measured along a line can be combined to one data set and are evaluated with fast FT-SAFT reconstruction calculation. Together with 3D imaging technique the scatterers and reflectors in the volume of interest can quickly be analyzed on site with cross and longitudinal sections as well as depth sections and phase evaluation (corresponding to ultrasonic B- and C-scans).

In Fig. 6.34 one practical application is presented as example. The aim was to verify if and where are tendon ducts inside of a cross girder, which is 60 cm thick. The data were measured along a line (length 1.16 m) with a step width of 2 cm (orientation of the array perpendicular to the measuring line). The result of the 3D-FT-SAFT reconstruction is shown in Fig. 6.34: the cuboid at the right (a) represents the reconstructed volume (surface: 0.40 m x 1.26 m, depth: 0,70 m). The other parts of the graph represent the different sections, which can be interactively adjusted by three planes. The measuring system with linear SAFT reconstruction also is distributed and applied as commercial equipment [Kozlov et al, 2006].

There are numerous reports on practical application of the Linear Scanner system with evaluation software for magnitude representation [De la Haza et al, 2008]. Here several 2D-SAFT evaluations of the array positioning perpendicular to the tendons are combined to one representation showing the reflection magnitude of the tendon duct.

In Figs 6.34a) to 6.34d) an application on a prestressed box girder bridge is presented [Rapaport, 2010]. There are four layers of tendon ducts in the girder, the upper layer has a concrete cover of 125 mm was measured step by step as described above (Fig. 6.34b).

In a section measured on the right border two tendons are imaged in the reconstructed SAFT-C-scan (Fig. 6.35d)): for tendon 5 (bottom) a high reflection

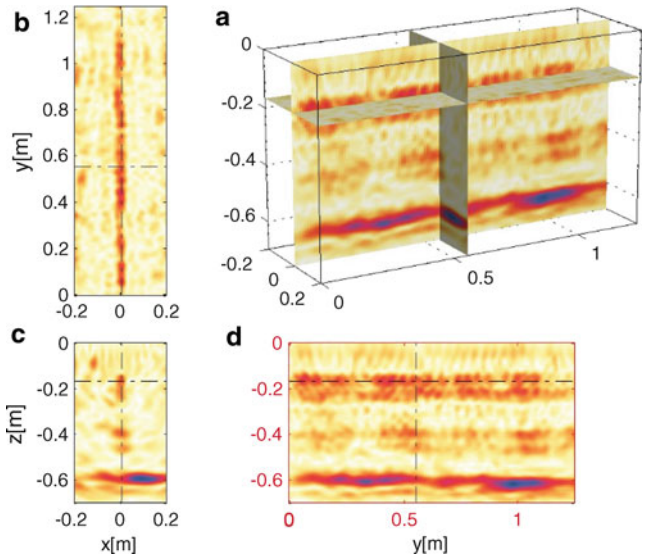

Fig. 6.34 Result of measurement at a cross girder measured with linear array and 3D imaging with FTSAFT: **a)** Cuboid of the reconstructed volume, three plains are selectable for the different sections: **b)** Depth section (C-scan), **c)** Cross section (B-scan parallel x), **d)** Longitudinal section (B-scan parallel y)

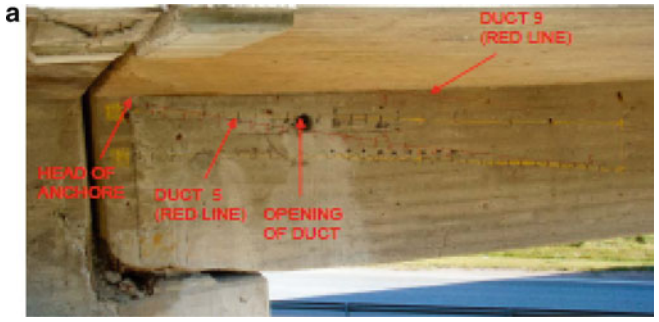

Fig. 6.35a) Investigation area at prestressed concrete bridge. Concrete cover of first layer of tendons: 125 mm

Fig. 6.35b) Positioning of linear array

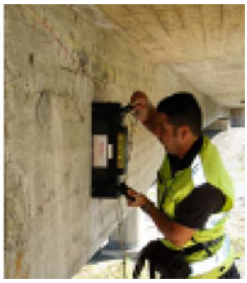

Fig. 6.35c) Verified grouting fault at duct 5

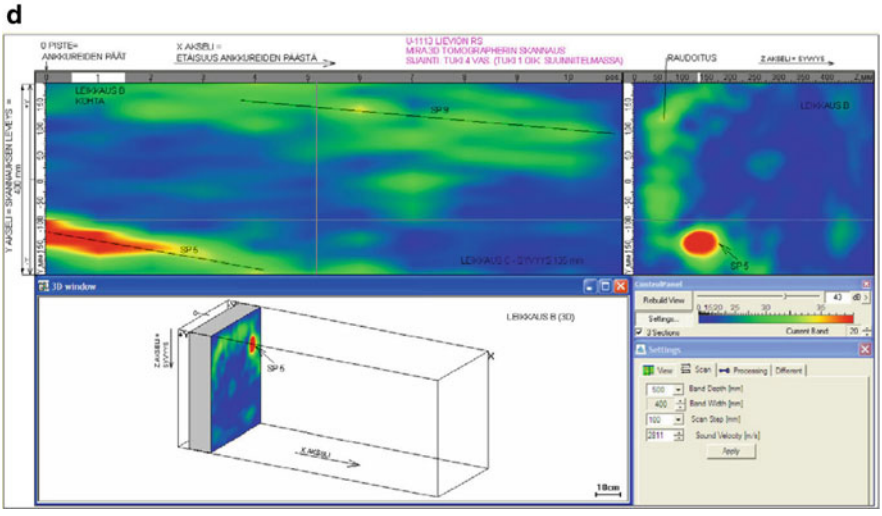

Fig. 6.35d) Magnitude representation of duct 9 (top) and 5 (bottom) of right (right border of measuring area shown in Fig. 6.35a)

magnitude relative to duct 9 (top) is measured indicating bad grouting conditions. This was verified by opening duct 5 (photograph Fig. 6.35c)) and endoscopy. At other locations of the same bridge it was verified that a duct showing similar reflectivity as duct 9 was well grouted.

6 Ultrasonic Through Transmission

Ultrasonic through transmission is frequently applied in order to measure (determine) the elastic parameters of building materials. From ultrasonic velocity of pressure waves and shear waves the elasticity modules and Poisson's ratio can be calculated.

The distribution of ultrasonic velocity in a building element may give basic information about its integral homogeneity and integrity. The velocity is influenced by the composition of the material as well as by heterogeneities, voids, deteriorated areas, and moisture. By measuring the distribution of the velocity such areas can be localized and classified.

There are several possibilities of ultrasonic through transmission tests. The simplest one is measuring the direct transit time with ultrasonic transmitters positioned directly opposite to the receiver. Other methods are adapted from the crosshole sonic logging method, where two transducers are positioned step by step along lines at both sides of the building element ([Olson and Hollema, 2003], [Binda et al, 2001]). Thus e.g. the velocity distribution in the wall can be roughly deduced. These methods are restricted for the application of coplanar surfaces.

A more sophisticated method is the calculation of the velocity distribution by means of tomographic calculation, based on an inversion applying the so called Radon-transformations. From this, generally an accurate image of the velocity distribution in the inner of the investigated object can be deduced and is imaged in corresponding slices. This method is widely used in metal and plastic investigation as well as medical application [Wüstenberg et al, 2008]. In building engineering this technique was recently developed for masonry (bricks and natural stones) [Wendrich et al, 2006].

Typical ray path examples are depicted in Figs. 6.36a) and 6.36b) for 4-sided and 2-sided access. In the latter also diffraction is taken into account. A principally difficulty for tomographic reconstruction in through transmission arrangement is that voids are regions of quasi zero transmission (c is nearly equal to zero). The convergence criterion of the algorithm is less distinct in this case.

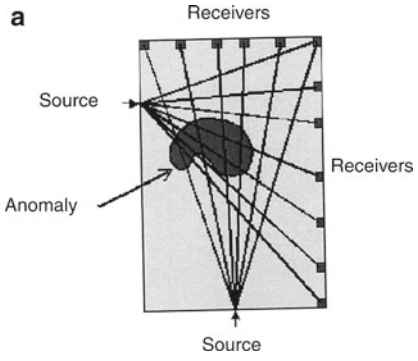

Fig. 6.36a) Ray path scheme for 4-sided access of transducers

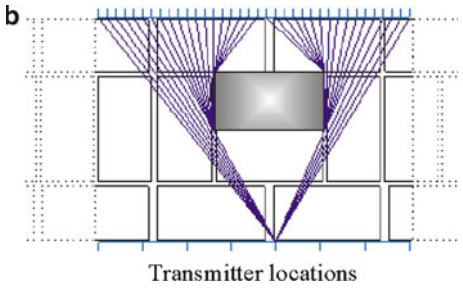

Fig. 6.36b) Ray path scheme for 2-sided access with void (application for masonry)

For concrete ultrasonic tomography is not used rather often. One example is detecting voids and honeycombing in concrete columns in the frequency range 100 kHz to 200 kHz [Schickert, 2004].

For prestressed concrete structures, tomographic surveys of different concrete beams are described in the British Advice Notes [Forde, 2006]. Examples are shown, where voiding in ducts is clearly detected by ultrasonic tomography and verified by impact-echo.

An application at a concrete bridge girder is described in [Martin et al, 2001]. Two test beams were examined: a 10 m long beam at the Transport Research Laboratory (TRL), Crowthorne, UK and a short test beam constructed at Stanger Science and Environment, Elstree, UK. The ducts were 40 mm in diameter in the first test and 100-mm diameter in the second one.

As example the result of a beam from the second test is shown in Fig. 6.37. The beam is 750 mm deep (the plan of the beam is given at the lower part of Fig. 6.37). The measuring field is 400 mm wide with grid locations at 100 mm spacing - using all four faces. A voiding is indicated by a low velocity. Apparent areas of low velocity in the corners are due to the reduced number of transit paths producing unreliable results. It has to be noted that edge effects or errors occur when there is a corner or low density of transmission/reception rays in a model. Edge effects or errors are highlighted in the cross-sections. The method is somewhat time consuming and so should be used in conjunction with a simpler testing method, e.g. sonic impact-echo, which identifies areas of interest. The smaller the ducts to be investigated, the smaller the required distances between testing stations. This therefore significantly increases the testing time.

7 Other methods

7.1 Radar for plastic ducts

For analysing steel tendon ducts radar is not suitable because shielding of electromagnetic waves. In contrast it is possible to apply Radar in case of post tensioned structures using tendon ducts made of plastic.

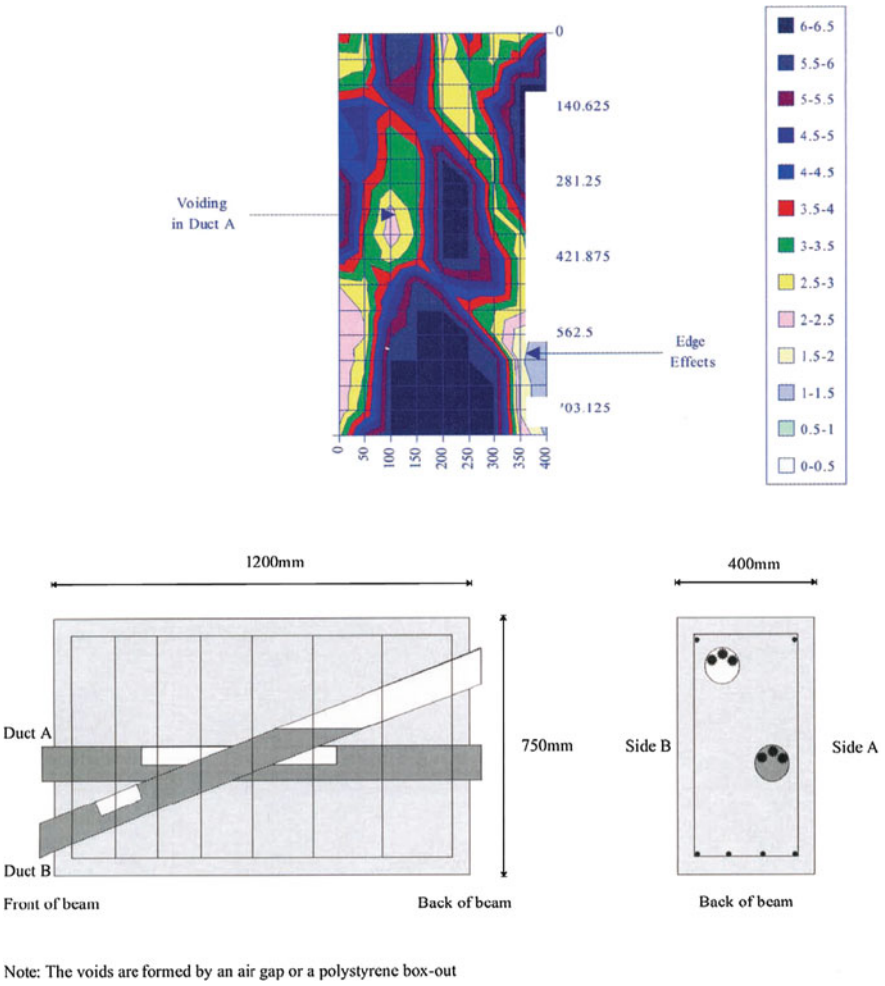

Fig. 6.37 Tomographic Survey of a cross-section of a concrete beam (after [Martin et al, 2001])

Radar Antennas in the frequency range of 500 MHz, 900 MHz and 1.5 GHz were tested at test specimens containing plastic tendon ducts of 90 mm and 63 mm diameter in beams made from concrete with maximum aggregate size of 20 mm [Forde, 2006]. As depicted in Fig. 6.38 the voided part of the duct (concrete cover 230 mm) is imaged showing a time of flight of t = 4 ns. Otherwise the reinforcing bars put in the specimen (spacing 20 mm) cause quite intense reflection of Radar pulses, which might hinder the image of the voided duct. Theoretical calculations lead to the conclusion that the perpendicular polarisation is more sensitive to the imaging of the voided plastic duct than the parallel orientation.

Ground-penetrating radar (GPR) inspection was conducted on fourteen concrete specimens by [Pollock et al, 2008]. Based on the GPR surveys conducted in this

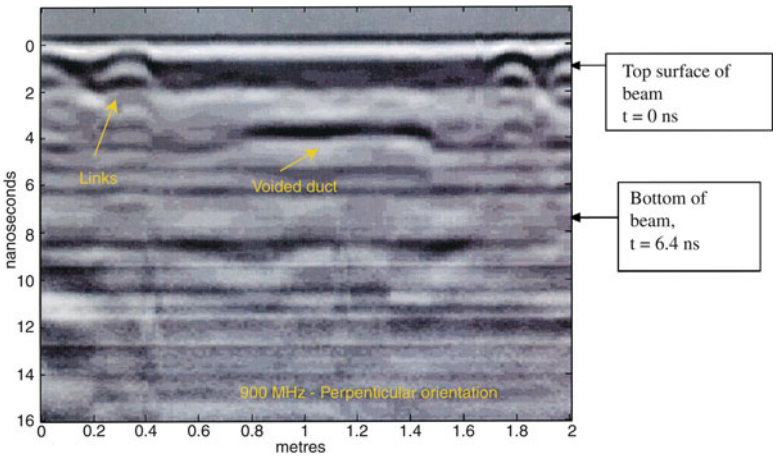

Fig. 6.38 Indication of voided plastic duct by means of 900 GHZ antenna (test specimen)

study, it is apparent that the detection of simulated voids within grouted ducts embedded in concrete is possible with a 1.5 GHz GPR system. Although none of the post-tensioning strands and simulated air voids within the grouted steel ducts was detectable, simulated voids within plastic ducts were generally detectable in GPR images. In another study [Conner et al, 2006], GPR was successfully used as a local inspection technique to precisely locate simulated voids as small as 1.5 *in*. (thick) adjacent to post-tensioning strands in grouted HDPE (High Density Polyethylene) ducts embedded in concrete slabs at depths of 5 to 20 centimeters.

7.2 Active Thermography

Thermal imaging can be used to detect simulated air voids within grouted post-tensioning ducts, thus locating areas where the post-tensioning steel strands are vulnerable to corrosion. [Pollock et al, 2008] prepared specimens with voids. For the thermal imaging inspections, six concrete specimens were constructed to simulate the walls of post-tensioned box girder bridges. The most important deduction taken from these inspections was that ducts and simulated voids were more detectable in the 20 cm thick specimens than in the 30 cm thick specimens. Inspections revealed the majority of the simulated voids in the former case, while, only one thicker specimen inspection indicated the presence of simulated voids (out of four voids in two ducts). Also, ducts were much clearer and visible in the thermal images of the thinner specimens.

[Rieck and Hillemeier, 2003] used transient thermography to monitor the grouting of steel ducts. All voids in the ducts could be detected using the heat of hydration of the cement lime inside the ducts. Even voids in tendons with a concrete

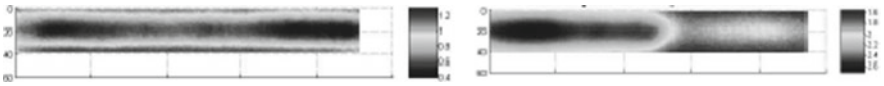

Fig. 6.39 Phase image of the beam without (left) and with (right) defect, at 0.78 mHz (after [Brachelet and al, 2009])

cover of 12 cm could be detected at an early stage. Applying thermal impulse heating and IR imaging for the same specimen, the voids in the tendon ducts could be localized up to a concrete cover of 7 cm.

Another heating source was used by [Brachelet and al, 2009], which consisted in induction heating, with a magnetic field. The analysis of both magnitude and phase on thermal images has shown that it is possible to identify the ungrouted areas (Fig. 6.39). The major drawback remains the relative slowness of the procedure. Further studies should focus on the design of the inductor and the heating time optimization.

Up to now, transient IR thermography for localizing grouting faults was mainly developed in laboratory, but very little on site application is reported. The contact-free aspect of this method is very attractive, when rapid measurements are desired. Although this method is very powerful for testing materials such as steel and carbon fibre laminates, the maximum penetration depth in concrete seems to be limited to only about 100 mm.

8 Conclusions

Most applications concerning non-destructive testing of tendon ducts deal with metal ducts. Because of the shielding of electromagnetic waves off metal surfaces, radar is principally not applicable in this task. It can however be used in a first step, to locate the ducts on which other methods are applied.

Radiography applying X- and Gamma Radiation is the oldest method to investigate the interior of steel and concrete structures. They still play an important role for NDT of post tensioned concrete bridges because of the capability of penetrating thick concrete elements up to 1 m. Using digital imaging plates instead of films these methods have become much more sensitive during the last decade.

Principally the method requires that the building element is accessible from both sides. Using radioactive radiation sources the thickness is limited to about 0.7 m, applying linear accelerators (or betatrons) even a thickness up to 1 m is feasible with a acceptable expenditure of time.

The first applicable **mechanical wave** method applied for this purpose was Impact Echo. The first version of Impact-Echo, developed at the end of 1980s, involves equipment which is not too complex and rather easy to use. Impact-Echo was widely applied in the 1990s and had the advantage of dry coupling on concrete surfaces. Even though evaluation in the frequency domain works best for planar slabs, the method was also applied for post tensioned structures with more complicated

geometry. Since mid-1990s, several commercial equipments came into the market and numerous applications were reported with partially verified results.

Basic research on this method at the beginning in the 1990s showed that the geometry of building elements affects the signals recorded. Based on principles of multiple reflections at tendon ducts, other concepts such as back wall frequency shift and influence of stiffness were thoroughly investigated. The originally affirmed reduction of Impact-Echo frequency to its half in case of metallic reflection could never be confirmed for grouted tendon ducts.

The principle of impact echo imaging deduced from 2-D measurements was developed and produced representations in analogy to ultrasonic evaluation (B-scan or Impact-Echogram according to longitudinal or cross section, respectively; C-scan according to depth section). However technical disputes on how to characterize the condition of tendon ducts remain.

Due to the advances in 2-dimensional Impact-Echo measurement, partly as a result of automated scanning systems used since 2003, the point measurement evaluation for tendon duct characterisation has become less common. At the same time modelling of wave propagation gained importance for interpreting the data and clarifying the results. For the theoretical background of Impact-Echo the aspect of Lamb waves published in 2005 was very important.

SIBIE (Stack Imaging of Spectral Amplitudes) is a new analysis scheme for impact echo based on spatial summation of the first and second harmonics. However real-world applications of SIBIE to characterize tendon ducts have not yet been reported.

The **ultrasonic echo** technique for evaluation of concrete elements has been developed in 3 phases:

In the 1990s broadband transducers in the appropriate frequency range (around 100 kHz) were developed. Simultaneously Synthetic Aperture techniques for imaging and modelling via Elastodynamic Finite Integration Techniques (EFIT) were developed and first applications on structures took place. Contactless measurement with laser interferometer was also used.

With the development of dry contact shear wave transducers in 2000, large areas could be measured much faster than before. This development also facilitated the construction of automated scanners for large structure evaluation (up to 40 m^2). Also new reconstruction programs and modelling of wave propagation helped further advancement and application of ultrasonic imaging. Several types of multistatic measuring equipment were developed and commercial NDT-testing of post tensioned concrete members began.

Since 2005, when the phase evaluation of the reflected signal was integrated in reconstruction calculation, the evaluation of testing results became more reliable. Validation and development of commercially available scanning systems in recent years has drawn a lot of attention.

More precise measuring capacities give rise to new questions. For example it is not yet completely understood how elastic waves penetrate or circulate around tendon ducts depending on their inner condition. Another point is the possibility to investigate the condition of tendon ducts in the second or third layer. The research work in such areas has only begun.

Nevertheless the potential of the method is rather promising leading to further research and development of equipment. The capability seems to be limited only by poor surface conditions or dense reinforcing layers.

Impact-Echo and ultrasonic echo field measurements have revealed very impressive results. Since dry contact transducers are also available for ultrasonic measurement in the appropriate frequency range, ultrasonic echo is sometimes advantageous because it can provide a better spatial resolution.

The use of ultrasonic through transmission method for inspection of tendon ducts has not been documented in the past years since 2002. One difficulty could be that air filled areas correspond to very low velocity whereas algorithms for through transmission are more precise for regions with greater wave speed.

Radar measurements (for plastic ducts only) and transient IR thermography (mainly used on laboratory) are alternative solution. The contact-free aspect of IR thermography is very attractive, when rapid measurements are desired. However, the penetration depth (in the case of dense reinforcements) and the slow time response for thermography put practical limits for on site measurements.

In order to advance reliable application of all testing methods three points seem to be useful:

- Precise description of the methods and quantitative assessment of their potentials and limitations. Controlled test sites and setting benchmarks have been developed for this purpose but there are still shared experiments.
- Educating and developing training courses for NDT engineers.
- Persuading owners and stakeholders that NDT can reduce the lifetime costs through quality assurance.

The activities of RILEM TC INR-207 were part of these actions. Next step may be to update existing and work out new standards. All this may encourage more producers, developers and engineering offices to come into the market with new equipment, software and offers.

References

Abraham O., Cote P. (2002) Thickness Frequency Profile for the detection of voids in tendon duct. ACI Structural Journal 99, 3, pp. 239-247.

Abraham O., Cottineau L.M., Valade M., Bedaoui S., Argoul P. (2009) Laser interferometer robot for the detection of voids in tendon ducts with the impact echo method, Int. Conf. NDT-CE 2009, Nantes, France.

Abraham O., Popovics J., Cottineau L.M., Durand O. (2010) Laser ultrasonics for civil engineering: some applications in development for concrete non destructive testing, Int. Conf. Laser Ultrasonics, 2010, Bordeaux, France.

Abraham O., Popovics J. (2010) Non destructive evaluation of reinforced concrete. Chapter 21: impact echo, pp. 466-489, ed. Maierhofer C., Reinhardt H.W., Dobman G., Woodhead Publ. Ltd.

AFNOR (2001) NF A09-202 Non-destructive testing - General principles for radiographic examination of reinforced concrete and prestressing materials by X- and gamma.

Algernon D. (2007) Measurements at specimen in Lyon (CETE-LCPC), private comm..

Al-Qadi I., Washer G. (2006) NDE Conference on Civil Engineering, A Joint Conference of the 7th Structural Materials Technology: NDE/NDT for Highways and Bridges and the 6th Int. Symp. NDT-CE, 14.-18. August 2006, St. Louis, MO, USA, CD-ROM.

Alver N., Ohtsu M. (2006) Visual identification of defects in concrete by SIBIE procedure. In: Al-Quadi, I. and G. Washer (eds.); Proc. NDE Conference on Civil Engineering, 14-18. August 2006, St. Louis, MO, USA.

Alver N., Ohtsu M. (2007) BEM analysis of dynamic behavior of concrete in impact-echo test. Construction and Building Materials, Elsevier, Vol. 21, 3, pp. 519-526.

Alver N., Takaki K., Ohtsu M. (2007) Visual identification of surface-crack depth in concrete by SIBIE. JCA Proc. of Cement & Concrete (Japan Cement Association), Vol. 60, pp. 199-204.

Ata N., Mihara S., Ohtsu M. (2007) Imaging of ungrouted tendon ducts in prestressed concrete by improved SIBIE. NDT&E International 40, p. 258-264.

BASt (2010) http://www.bast.de/nn_82260/EN/e-Aufgaben/e-abteilung-b/e-referat-b4/e-schadensanalyse/e-schadensanalyse.html

Binda L., Saisi A. Tiraboschi C. (2001) Application of sonic tests to the diagnosis of damaged and repaired structures, NDT&E International 34, pp.123- 138.

Brachelet F., Du T., Defer D., Antczak E. (2009) Detection of poor filling in prestressed beams specimen by inductive thermography and transfer function analysis, NDTCE'09, Non-Destructive Testing in Civil Engineering, Nantes, France, June 30th – July 3rd, 2009

CETE (2006) Centre d'Etudes techniques de l'Equipement de Lyon, La Gammagraphie sur les ouvrages d'art.

Colla C., Schneider G., Wiggenhauser, H. (1999) Automated Impact-Echo: Method improvements via 2-D and 3-D imaging of concrete elements, In: Proceedings of Structural Faults and Repair, London, pp. 1-11.

Concrete Society, the (2002) Durable post-tensioned concrete bridges, Concrete Soc. Technical Report No. 47, Second Edition, Century House, Crowthorne, Berkshire RG45 6YS, UK.

Conner J.M., Pollock D.G., Khaleghi, B. (2006) Detection of Simulated Voids in Grouted Ducts using Ground-Penetrating Radar, Proc. 2006 Concrete Bridge Conference, Portland Cement Association

De la Haza A., Petersen C. G., Samokrutov A. (2008) Three dimensional imaging of concrete structures using ultrasonic shear waves, In: Forde, M. C. (ed.); Proc.12th Int. Conf. Structural Faults and Repair, Edinburgh, Scotland, 10.-12. Juni 2008.

DGZfP (2010) http://www.dgzfp.de/Fachaussch%C3%BCsse/ZfPimBauwesen.aspx

DGZfP (1990) 90DGZ1 Merkblatt für die Durchstrahlungsprüfung von Stahlbeton und Spannbeton (B1), Deutsche Gesellschaft für Zerstörungsfreie Prüfung e.V., Berlin.

Dufay J.C., Piccardi J. (1985) SCORPION, premier système de radioscopie télévisée haute énergie pour le contrôle non destructif des ouvrages d'art en béton précontraint », Bulletin de liaison des Laboratoires des Ponts et Chaussées, N°139, pp 77-84, Sep-Oct 1985.

Eichinger E. M., Diem J., Kolleger J. (2000) Bewertung des Zustandes von Spanngliedern auf der Grundlage von Untersuchungen an Massivbrücken der Stadt Wien. Institut für Stahlbeton und Massivbau, Heft 1.

FDoT (2003) Florida Department of Transportation Central Structures Office: Test and Assessment of NDT Methods for Post-Tensioning Systems in Segmental Balanced Cantilever Concrete Bridges. DMJM & HARRIS.

Forde M. (2006) Advice Notes NDT Highway Structures, GB, http://www.trl.co.uk/online_store/reports_publications/papers_articles/cat_paper_highway_engineering/.

Gibson A., Popovics J. (2005) Lamb Wave Basis for Impact-Echo Method Analysis. Journal of Engineering Mechanics, ASCE 5, pp. 438-443.

Große Ch., Beutel R., Wiggenhauser H., Algernon D., Schubert F. (2007) Impact-Echo. Bergmeister, K., Wörner, J.-D. (Hrsg.); BetonKalender 2007, Verkehrsbauten-Flächentragwerke. Berlin: Verlag Ernst & Sohn, Bd. 1, Kapitel V Echoverfahren in der zerstörungsfreien Zustandsuntersuchung von Betonbauteilen, Absch. 3, S. 496-505.

Helmerich R., Niederleithinger E., Algernon D., Streicher D., Wiggenhauser H. (2008) Bridge inspection and condition assessment in Europe, Transport. Res. Record, TRB, Vol 2044, pp. 31-38.

IAEA (2002) Guidebook on non destructive testing of concrete structures, Int. Atomic Eergy Agency, Vienna.

Jansohn, R. and J. Scherzer (2002) Improper filled ducts detected by ultrasound reflection, In: Proceedings of the 8th ECNDT, 17.-21. June 2002, Barcelona, Spain, CD-ROM.

Kozlov V.N., Samokrutov A.A., Shevaldykin V.G. (2006) Ultrasonic Equipment for Evaluation of Concrete Structures Based on Transducers with Dry Point Contact. In: Al-Qadi, I. and Washer G. (eds.); Proc. NDE Conference on Civil Engineering, 14.-18. August 2006, St. Louis, MO, USA, pp. 496-498.

Krause M., Bärmann R., Frielinghaus R., Kretzschmar F., Kroggel O., Langenberg K., Maierhofer Ch., Müller W., Neisecke J., Schickert M., Schmitz V., Wiggenhauser H., Wollbold F. (1997) Comparison of pulse-echo methods for testing concrete. In: NDT&E International Sonderheft, Vol. 30, 4, pp. 195-204.

Krause M., Wiggenhauser H., Krieger J. (2002) NDE of a Post Tensioned Concrete Bridge Girder Using Ultrasonic Pulse Echo and Impact Echo, Proc. Structural Materials Technology (SMT), NDE/NDT for Highways and Bridges Topical Conference, 10.-13. September 2002, The Westin Cincinnati, Cincinnati, OH, USA

Krause M., Mielentz F., Milmann B., Streicher D., Müller W. (2003) Ultrasonic imaging of concrete elements: State of the art using 2D synthetic aperture. In: DGZfP (ed.); Int. Symp. NDT-CE Berlin, Germany, September 16-19, 2003.

Krause M., Milmann B., Schickert M., Mayer K. (2006) Investigation of Tendon Ducts by Means of Ultrasonic Echo Methods: A Comparative Study. Proceedings of the 9th Eur. Conf. on NDT, September 25-29, 2006, Berlin: DGZfP, BB 103-CD, Tu.3.2.1.

Krause M., Gräfe B., Mielentz F., Milmann B., Friese M., Wiggenhauser H., Mayer K. (2008) Ultrasonic Imaging of Post-tensioned Concrete Elements: New Techniques for Reliable Localization of Grouting Defects. In: Alexander M. G., Beushausen H.-D., Dehn, F. and Moyo P. (eds.); Proc. Concrete Repair, Rehabilitation and Retrofitting II, ICCRRR 2008, 24.-26.11.2008, Kapstadt, CD-ROM, pp. 521-527.

Krause M., Milmann B., Mielentz F., Streicher D., Redmer B., Mayer K., Langenberg K.-J., Schickert M. (2008) Ultrasonic Imaging Methods for Investigation of Post-Tensioned Concrete Structures: A Study of Interfaces at Artificial Grouting Faults and its Verification. Journal of Nondestructive Evaluation, 27, pp. 67-82.

Krause M., Mayer K., Friese M., Milmann B., Mielentz F., Ballier G. (2011) Progress in ultrasonic tendon ducts imaging, In: Derobert, X. and O. Abraham (eds.);EJECE No 77, in print.

Kroggel O., Scherzer J., Jansohn R. (2002) The Detectability of Improper Filled Ducts with Ultrasound Reflection Techniques. http://www.ndt.net/article/v07n03/ kroggel/kroggel.htm, NDT.net 7, 3, No. 03,

Krüger M., Groβe C.U. (2006) Crack depth determination using advanced impact-echo techniques, ECNDT.

Langenberg K.J., Marklein R., Mayer K. (2002) Applications to Nondestructive Testing with Ultrasound, in E. R. Pike, P. C. Sabatier (eds.),Scattering: Scattering and Inverse Scattering in Pure and Applied Science, pp. 594-617, Academic Press, London, UK.

Langenberg K.J., Marklein R., Mayer K. (2009) Theorethische Grundlagen der zerstörungsfreien Materialprüfung mit Ultraschall, Oldenbourg Wissenschaftsverlag GmbH München.

Lanneau P. (1993) Mise en oeuvre de l'accélérateur linéaire portable MINAC pour des contrôles radiographiques de chantier, Revue pratique de contrôle industriel,, vol. 32, no182, pp. 40-43,

Lausch R., Wiggenhauser H., Schubert F. (2002) Geometrieeffekte und Hüllrohrortung bei der Impaktechoprüfung von Betonbauteilen - Experimentelle und modelltheoretische Ergebnisse. In: DGZfP-Jahrestagung 06.-08. Mai 2002 in Weimar, DGZfP-Berichtsband BB 80-CD, Plakat 34, Berlin (2002).

Lin Y., Lin K. (1997) Transient impact response of bridge I-girders with and without flaws. ASCE Journal of Bridge Engineering, 2(4), 131-138.

Maierhofer Ch., Krause M., Mielentz F., Streicher D., Milmann B., Gardei, A., Kohl Ch. Wiggenhauser H. (2004) Complementary application of radar, impact-echo and ultrasonics for

testing concrete structures and metallic tendon ducts. in: Proc. 83rd Annual Meeting Transportation Research Board of the National Academies, 11.-15. January 2004, Washington, D.C.

Martin, J., Broughton, K., Giannopolous, A., Hardy, M. and M. Forde: Ultrasonic tomography of grouted duct post-tensioned reinforced concrete bridge beams. NDT&E International 34 (2001), p. 107-113.

Mayer K., Langenberg K.-J., Krause M., Maierhofer Ch., Milmann B., Kohl Ch. (2006) Characterization of Ultrasonic and Radar Reflector Types in Concrete by Phase Evaluation of the Signal and the Reconstructed Image. In: Proc. 9th European Conference on NDT, September 25-29, 2006, Berlin: DGZfP, BB 103-CD, We.1.3.4.

Mayer K., Langenberg K.-J., Krause M., Milmann B., Mielentz F. (2008) Characterization of Reflector Types by Phase-Sensitive Ultrasonic Data Processing and Imaging, J. of Nondestructive Evaluation 1-3, 27, pp. 35-45.

Mayer, K., Milmann, B., Krause, M. und F. Mielentz (2008b) Methode zum Nachweis von Verpressfehlern in Spannbeton durch Phasenauswertung bei Ultraschallecho-Verfahren, ZfP-Zeitung 112 (2008) 12, S. 37-40

Ohtsu M., Watanabe T. (2002) Stack imaging of spectral amplitudes based on impact-echo for flaw detection. NDT&E International, Vol. 35, No. 3, pp. 189-196.

Olson L.D., Hollema D.A. (2003) Crosshole Sonic Logging and Velocity Tomography Imaging of Drilled Shaft Foundation, Int. Symp. NDT- CE 2003, Berlin.

Patent (2006) Patentanmeldung DE 10 2006 027 132.7: Verfahren zum Detektieren von Fehlstellen in Betonbauteilen, BAM, Bundesanstalt für Materialforschung und –prüfung, Universität Kassel. Anmeldetag: 02.06.2006.

Pollock D.G., Dupuis K.J., Lacour B., Olsen K.R. (2008) Detecting voids in prestressed concrete bridge using thermal imaging and ground penetrating radar, WA-RD 717.1, WSDot Res. Rep., dec. 2008.

Rapaport, G., inc. Ramboll, Finland: Scanning By MIRA 3D Tomographer, case study, 2010, unpublished.

Rieck C., Hillemeier B. (2003) Detecting Voids Inside Ducts of Bonded Steel Tendons Using Impulse Thermography. in: DGZfP (ed.); International Symposium Non-Destructive Testing in Civil Engineering (NDT-CE) in Berlin, Germany, September 16-19, 2003, Proceedings on BB 85-CD, P21, Berlin.

Roenelle P., Abraham 0. (2006) Détections de vides dans les gaines de précontraintes par la méthode écho, In: Abraham, O. (ed.), Champs physiques et propagation dans les sols et les structures du génie civil, ISSN 1167-4865, LCPC, pp. 81-93.

Sansalone M., Streett W. (1997) Impact-Echo. Jersey Shore, PA: Bullbrier Press.

Schickert M., Krause M., Müller W. (2003) Ultrasonic Imaging of Concrete Elements Using Reconstruction by Synthetic Aperture Focusing Technique. Journal of Materials in Civil Engineering (JMCE), ASCE Vol. 15, 3, pp. 235-246.

Schickert M. (2004) Ultraschall-Tomographie an Betonbauteilen, in: DACH-Jahrestagung, 17-19 may 2004, Salzburg.

Schickert M. (2005) Progress in ultrasonic imaging of concrete. Materials and Structures 38; 11, pp. 807-815

Schickert, M. and M. Krause (2010) Ultrasonic evaluation of reinforced concrete structures, in: Maierhofer, Ch., Reinhardt, H.-W. and G. Dobmann (eds.): Non-destructive evaluation of reinforced concrete structures, Woodhead Publishing Limited, Cambride, Part II.22, pp. 490-530

Schubert F., Köhler B. (2008) Ten lectures on Impact-Echo. Journal of Nondestructive Evaluation 27, 1-3, pp. 5-21.

Sodeikat Ch., Dauberschmidt Ch. (2008) Anwendung von Georadar und Ultraschall – Fallbeispiele aus der Praxis eines Ingenieurbüros. In: Tagungsband zur Fachtagung Bauwerksdiagnose 2008, Praktische Anwendungen Zerstörungsfreier Prüfungen und Zukunftsaufgaben, 21.-22.02.2008, Berlin, Berichtsband BB 112-CD, Vortrag 13.

Streicher D., Algernon D., Wöstmann J., Behrens M., Wiggenhauser H. (2006) Automated NDE of post tensioned bridge using imaging echo methods, ECNDT, Berlin, 25-29 Sept. 2006.

Taffe A., Borchardt K., Wiggenhauser H. (2003) Specimen for the improvement of NDT-methods - Design and construction of a Large Concrete Slab for NDT methods at BAM. In: DGZfP (ed.); Int. Symp. NDT-CE.

Taffe A., Kind T., Stoppel M., Wiggenhauser H. (2008) OSSCAR - Development of an On-Site SCanneR for automated non-destructive bridge testing. In: Alexander M. G., Beushausen H.-D., Dehn,F. and Moyo P. (eds.); Proc. Concrete Repair, Rehabilitation and Retrofitting II, ICCRRR 2008, 24.-26.11.2008, Kapstadt, CD-ROM, pp. 541-545.

Tinkey Y., Olson, L., Wiggenhauser H. (2005) Impact Echo Scanning for Discontinuity Detection and Imaging in Post tensioned Concrete Bridges and Other Structures. Materials Evaluation 63, 1, pp. 64-69.

Tinkey Y., Olson L.D. (2008) Application and Limitations of Impact Echo Scanning for Void Detection in Post tensioned Bridge Ducts, Transport Research Record: Journal of the Transportation Research board No. 2070, Washington, D.C., pp. 8-12.

Vogel T. (2002) Zustandserfassung von Brücken bei deren Abbruch - Erkenntnisse für Neubau und Erhaltung. Bauingenieur 77, 12, 559-567.

Wendrich A., Trela C., Krause M., Maierhofer C., Effner U., Wöstmann J. (2006) Location of voids in masonry structures by using radar and ultrasonic traveltime, ECNDT, Berlin.

Wiggenhauser H., Schickert M. (2003) Non-destructive Testing in Civil Engineering, Proceedings Berlin 2003

Wiggenhauser, H. (2003) Duct inspection using scanning impact-echo, In: DGZfP (Ed.); International Symposium Non-Destructive Testing in Civil Engineering (NDT-CE) in Berlin, Germany, September 16-19, 2003, Proceedings on BB 85-CD, V101, Berlin (2003).

Wiggenhauser H., Streicher D., Algernon D., Wöstmann J., Behrens M. (2007) Automated Application and Combination of Non-Destructive Echo Methods for the Investigation of Post-Tensioned Concrete Bridges. In: Long, A. and J. Bungey (eds.); Proceedings of Concrete Platform, Belfast, 19.-20.04.2007, Proc. and CD-ROM, pp. 261-270.

Wüstenberg H., Erhard A., Austel W., Klanke H.P. (1988) Ultrasonic echo tomography. A new procedure for defect presentation. Ultraschall- Echo- Tomographie, ein neues Verfahren für die Darstellung von Fehlern. Konferenz- Einzelbericht: Pressure Vessel Technology. 6th Int. Conf., pp1481 – 1492, Oxford: Pergamon Press.

Zhu J., Popovics J. (2007) Imaging Concrete Structures Using Air-Coupled Impact-Echo. Journal of Engineering Mechanics, ASCE, 6, p. 628-640.